N73-12840

NASA TECHNICAL
MEMORANDUM

NASA TM X-64690
August 1972

NASA TM X-64690

CHEMICAL PROPULSION RESEARCH AT MSFC

RESEARCH ACHIEVEMENTS REVIEW

VOLUME IV REPORT NO. 6

SCIENCE AND ENGINEERING DIRECTORATE
GEORGE C. MARSHALL SPACE FLIGHT CENTER
MARSHALL SPACE FLIGHT CENTER, ALABAMA

ENGINEERING ADVANCES IN AEROSPIKE ROCKET ENGINES

By

Rex Bailey

INTRODUCTION

In a conventional bell nozzle engine, thrust is produced by the expansion of combustion gases within the confines of the nozzle wall. The magnitude of the thrust varies in accordance with the equation shown in Figure 1. For high altitude engine operation, it is generally desirable to maximize nozzle exit velocity, which requires that large nozzle area ratios be used. Operation of high area ratio nozzles at low altitudes, however, typically produces a nozzle exit pressure lower than ambient pressure, which results in a reduction of thrust. Maximum thrust generation at both low and high altitudes can result only if the effective nozzle area ratio varies with altitude such that nozzle exit pressure remains equal to ambient pressure, a characteristic called altitude compensation. The advantages of an altitude compensating nozzle in comparison to a high area ratio bell nozzle are qualitatively shown in Figure 1.

The spike nozzle concept shown in Figure 2 was conceived as a means of achieving altitude compensation. Combustion gases are generated within a toroidal chamber, exhausted through an annular throat, then expanded against a spike nozzle. Since the outer free-jet boundary of the combustion gases is controlled by ambient pressure, overexpansion of the gases cannot occur and the nozzle is altitude compensating to the area ratio limit of the particular design. An aerospike nozzle, also shown in Figure 2, operates in a similar manner except that the lower part of the spike nozzle is removed and an aerodynamic spike formed by a flow of gases through the nozzle base is substituted.

The aerospike nozzle concept had, in addition to altitude compensation, other desirable features when compared to an equivalent bell nozzle: it had the potential of requiring a thrust chamber length only 15 to 20 percent as long; it could be gimballed within a much smaller envelope; and larger area ratios and

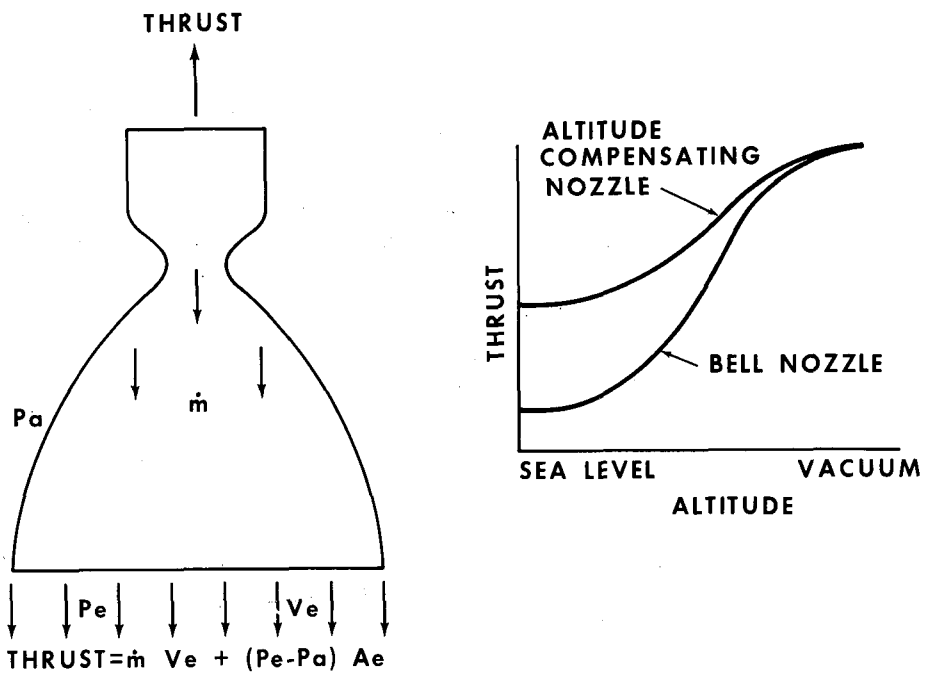

Figure 1. Rocket nozzle characteristics.

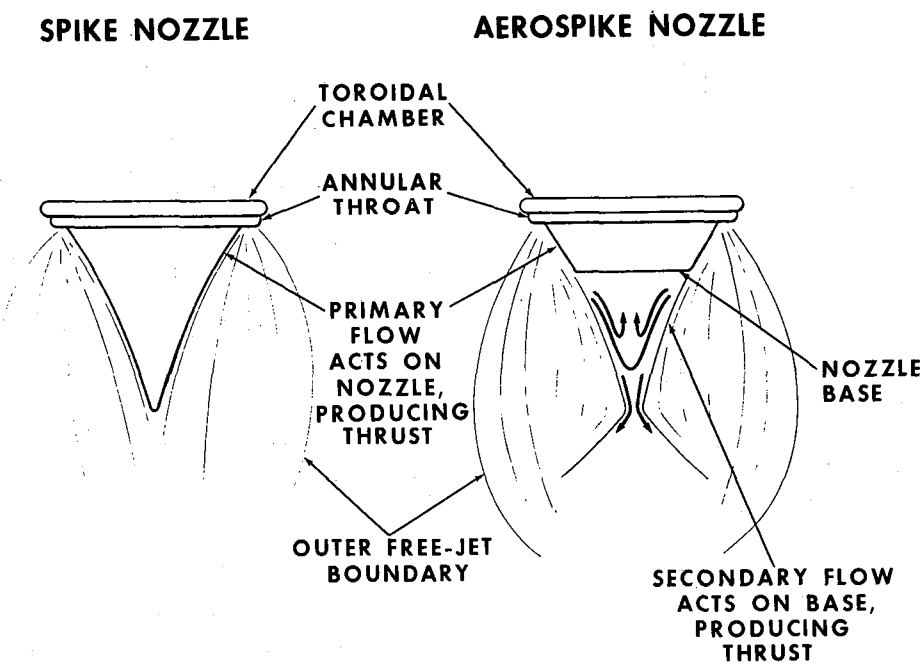

Figure 2. Altitude compensating nozzles.

higher vacuum performance could be achieved by using the entire base area of a stage. Several potential problem areas were also identified as being unique to the aerospike nozzle. Obtaining complete combustion within a short toroidal chamber was a new requirement to be demonstrated. Combustion stability was uncertain from the standpoint of both acoustic stability and feed system dynamics. Thrust chamber cooling was considered more difficult because of larger surface area requirements and the associated complexity of regenerative heat exchangers. To investigate these potential advantages and disadvantages, the Advanced Engine Aerospike (AEA) program was initiated.

ADVANCED ENGINE AEROSPIKE PROGRAM

The Advanced Engine Aerospike program was undertaken to satisfy the following objectives:

1. To demonstrate combustion efficiency.

2. To demonstrate aerospike nozzle performance.

3. To evaluate steady-state and dynamic operation of a full size thrust chamber.

4. To evaluate combustion stability.

5. To demonstrate regenerative cooling of combustor and nozzle walls.

The baseline engine cycle concept used for study purposes is shown in Figure 3. In this cycle, hot gases are extracted from the main combustion chamber and used to drive the fuel and oxidizer turbines. The gases are then expelled through the base of the nozzle to enhance nozzle performance.

The basic thrust chamber design used for the Advanced Engine Aerospike program is shown in Figure 4. The chamber was rated at 1.1 MN (250 000 lb) thrust at a chamber pressure of 10.34 MN/m^2 (1500 psia) using liquid oxygen and liquid hydrogen as propellants. The thrust chamber diameter was 254 cm (100 in.). The injector elements were unlike triplets having two fuel streams impinging on one oxygen stream. Three combustion chambers were fabricated. The first chamber was a solid-wall, uncooled configuration that was used

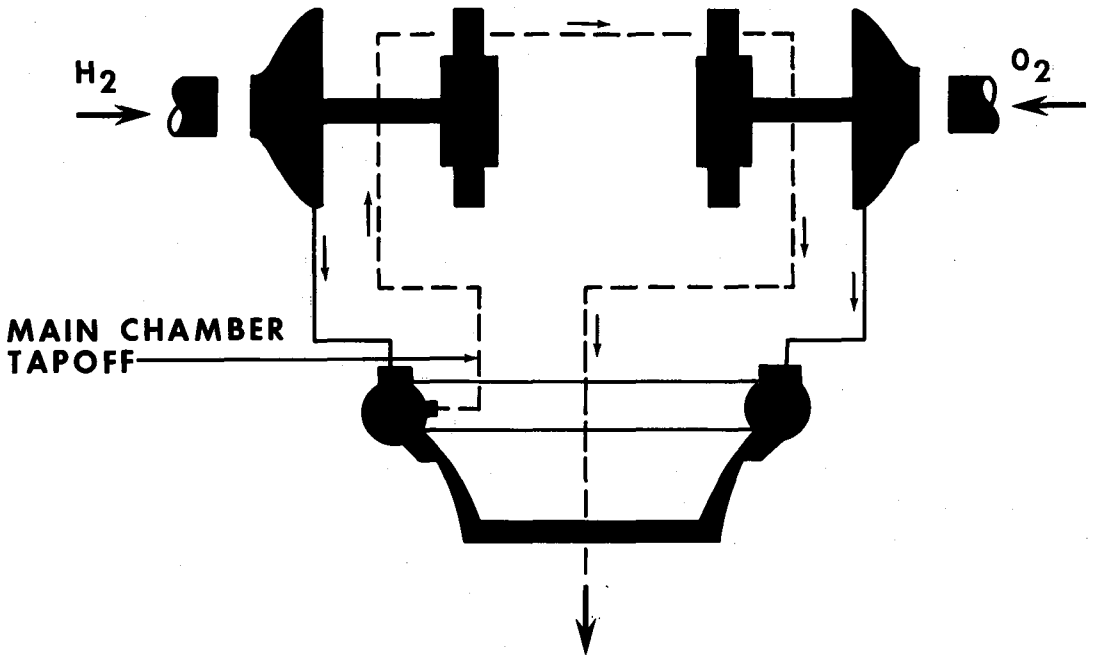

Figure 3. Aero-tapoff engine cycle.

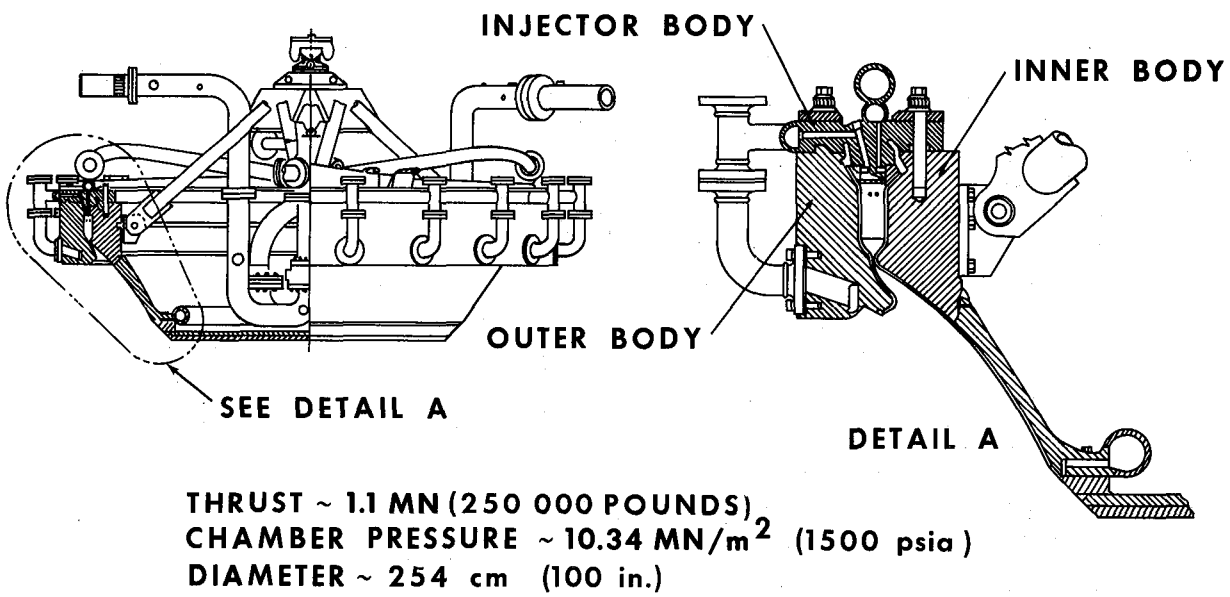

Figure 4. Aerospike tube wall thrust chamber.

for injector checkout. The two additional thrust chambers were fuel regeneratively cooled by using tube bundle heat exchangers. Stainless steel tubes were used for one chamber and nickel tubes for the other. Each assembly required approximately 6000 tubes which were tapered to a diameter of approximately 2.0 mm (0.078 in.) at the nozzle throat. Because of the large number of very small tubes, fabrication of the cooled chambers proved to be difficult. Both solid and porous base plates were used to control base bleed flows.

Testing was initiated using the solid-wall chamber in a system-and-dynamics investigation. This effort was conducted to determine the thrust chamber transient and low frequency stability characteristics. As shown in Figure 5, servocontrol throttle valves and dump valves were used for the simulation of various turbopump and start configurations. By properly sequencing these valves, an indication of turbopump stall margin was obtained.

Testing of the cooled chambers was conducted at both sea level and simulated altitude to obtain performance data. A sea level test firing photograph is shown in Figure 6. A total of 34 firings was conducted, yielding 74 test data points with a total accumulated test duration of 133 s. Chamber pressures ranged from 1.4 to 7.3 MN/m^2 (200 to 1055 psia) with propellant mixture ratios from 2.0 to 5.0. Base bleed hydrogen flow rates were 0, 0.4, and 2.2 percent of total propellant flow rate.

A comparison of test data with predicted performance is shown in Figure 7. It can be seen that the agreement was generally very good. The achieved altitude compensation as compared to the equivalent bell nozzle predicted performance is also evident. The conclusions were reached that high performance was achievable with aerospike nozzles and that the performance achieved through altitude compensation was predictable. Because of difficulties encountered during the fabrication and test efforts, it was also concluded that combustion chamber compartmenting rather than injector baffles should be used for combustion stability, and that nontubular thrust chambers should be investigated to simplify the fabrication processes.

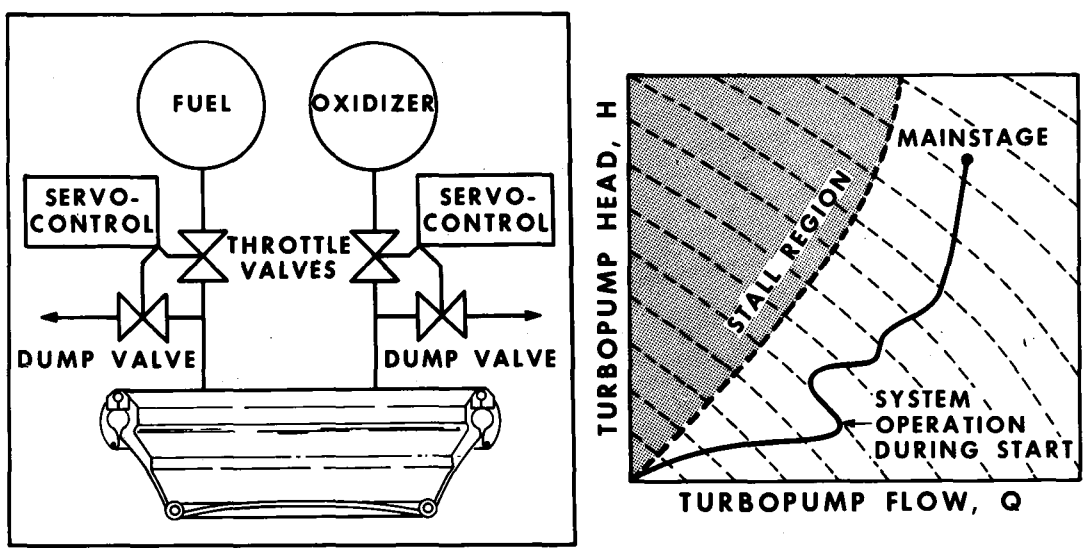

- SIMULATION OF VARIOUS START CONFIGURATIONS (TANK HEAD, GAS-SPIN, TAP-OFF, WARM ENGINE, ETC)
- SIMULATION OF VARIOUS TURBOPUMP CONFIGURATIONS (CENTRIFUGAL, AXIAL, HYBRID, ETC)

Figure 5. Aerospike system-and-dynamics investigation — simulated system transients.

COMPONENT TECHNOLOGY

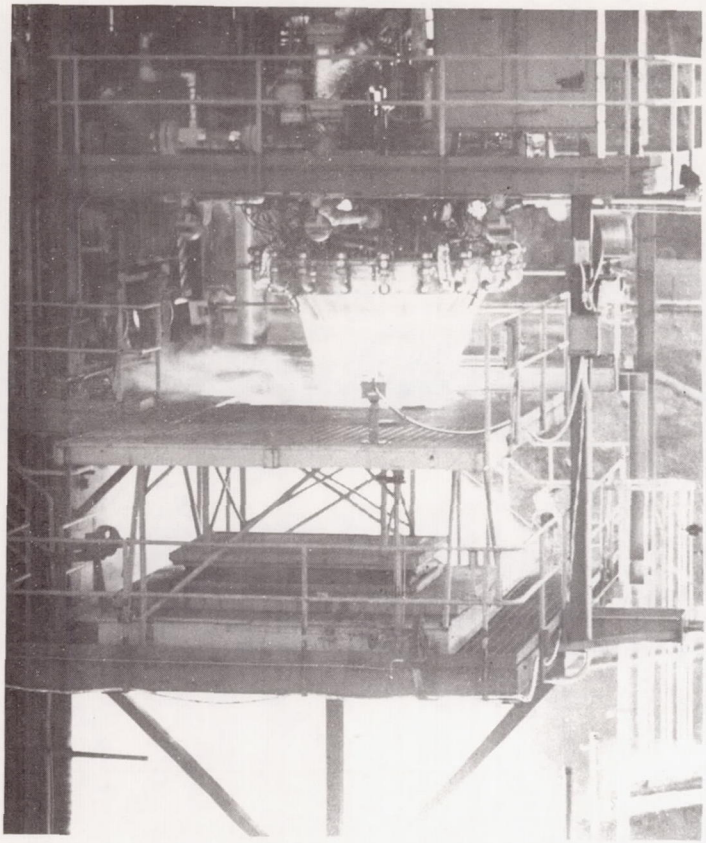

Figure 6. Aerospike thrust chamber firing.

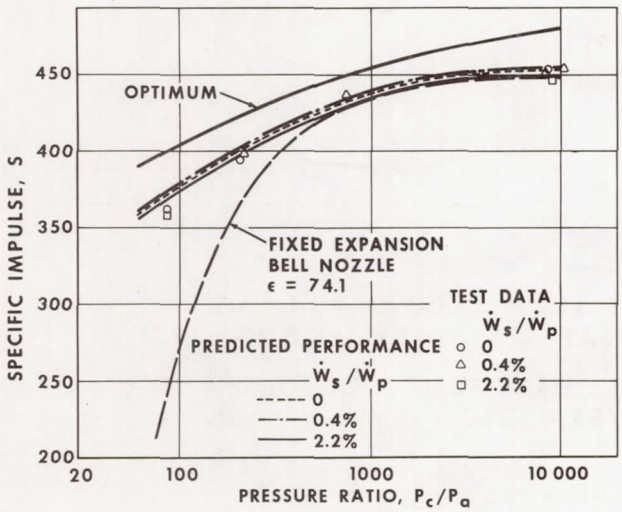

Figure 7. Specific impulse versus pressure ratio for MR = 5.0 .

Segment testing was conducted using hardware of the type shown in Figures 8 and 9. Copper combustion chamber side panels were machined to form variable depth cooling channels in the outer sides. Thin sheets of stainless steel were brazed to the copper lands to close out the channels and form the coolant passages. The panels were then stamped to the desired chamber contour. Copper end plates having drilled coolant passages closed the ends of the combustion chambers, and installation of the injector completed the assembly. Segments of this type were tested at chamber pressures ranging from 2.35 to 14.2 MN/m^2 (340 to 2045 psia) and propellant mixture ratios from 5.7 to 6.3. These tests indicated the feasibility of milled channel construction as a means of chamber segment fabrication. Additional efforts were conducted to establish injector and combustor geometry effects on combustion performance. Combustor lengths ranging from 5.0 to 14.5 cm (2.0 to 6.0 in.) and widths from 2.54 to 5.08 cm (1.0 to 2.0 in.) were tested using both impinging jet and concentric orifice injectors. Data from these tests are summarized in Figure 10 and indicate that impinging jet injectors produce higher combustion performance for chamber lengths less than 13 cm (5.2 in.). For chamber lengths greater than this, both types of injectors performed at nearly 100 percent efficiency. Combustor length rather than characteristic length, L^*, was found to be the primary geometric parameter affecting performance.

In support of the original goal to use thrust chamber tapoff gases for turbine drive, an effort was conducted to determine the feasibility of extracting tapoff gases through the main injector face. One of the two injector configurations tested is shown in Figure 11. The main injector was a standard concentric tube design with a single tapoff port placed in the center of the face. Several main injector elements in the area surrounding the tapoff port operated at a fuel-rich mixture bias to provide the desired temperature for the tapoff gases. A test series of 24 firings was conducted, and it was determined that injector face tapoff is a satisfactory method of providing turbine drive gases.

As the aerospike technology efforts continued to progress, it became increasingly evident that a building block approach to aerospike engine development and fabrication was desirable. This concept is outlined in Figure 12. By segmenting the combustion

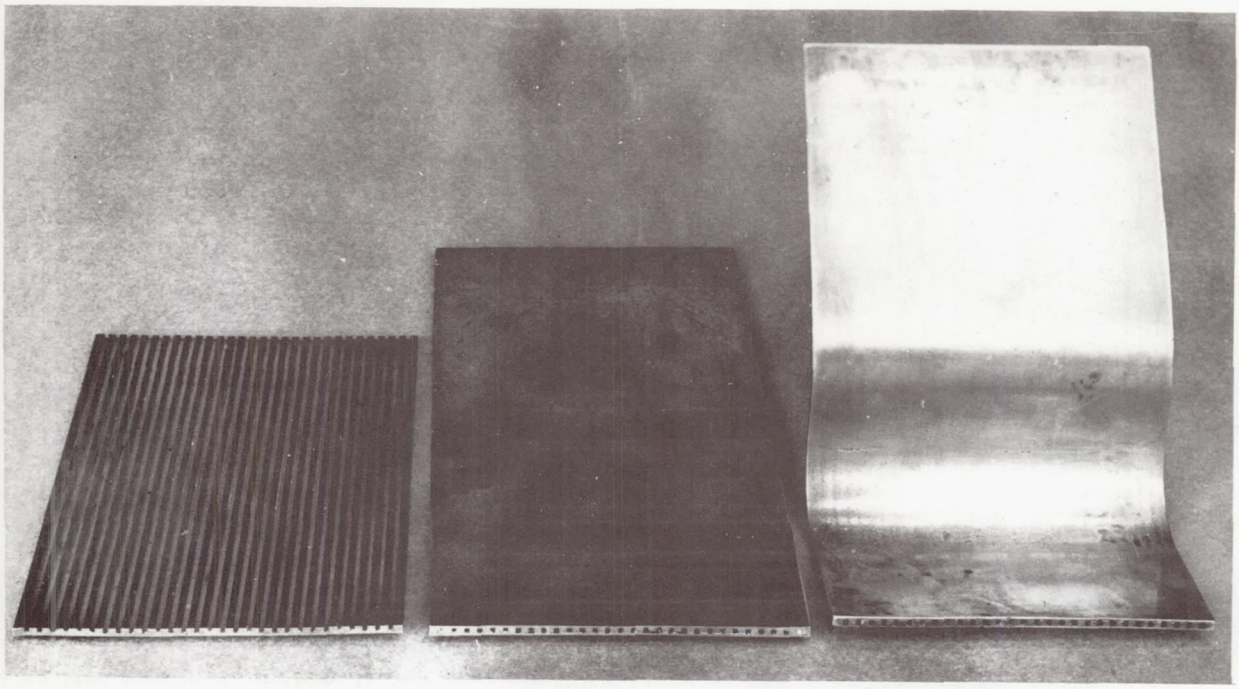

Figure 8. Milled slot chamber panels.

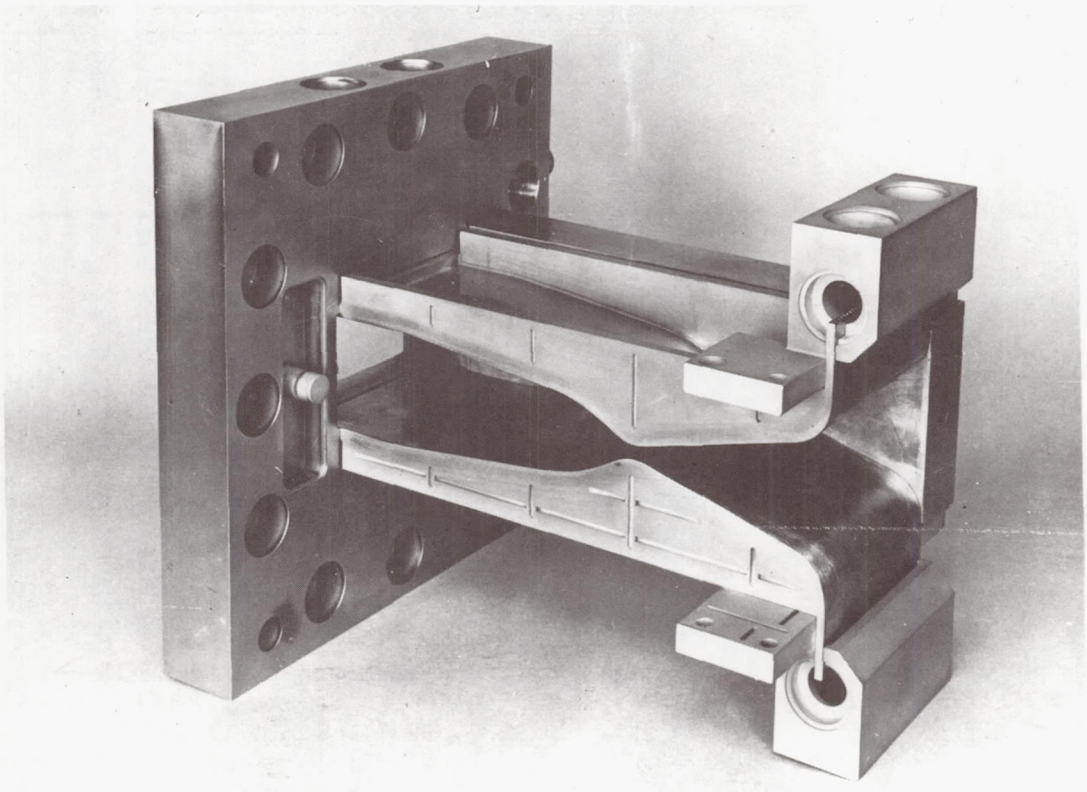

Figure 9. Milled slot chamber segment.

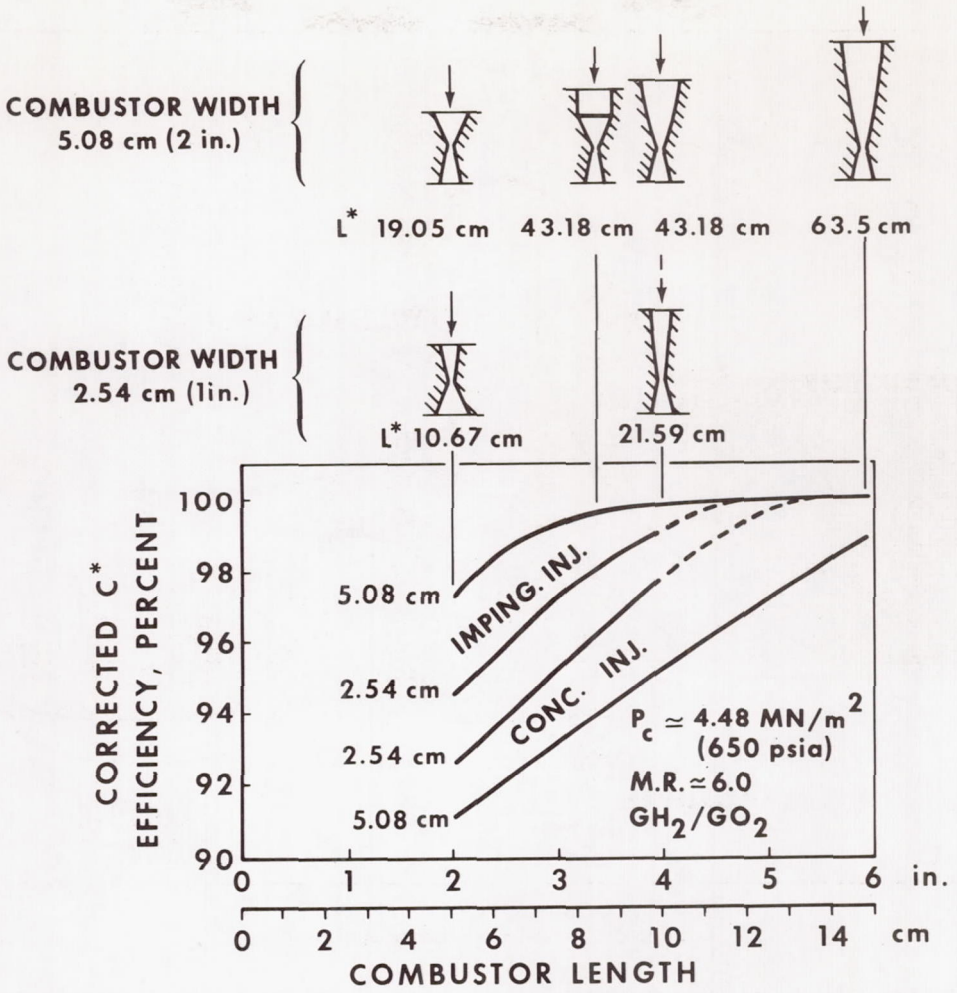

Figure 10. Combustor geometry effects.

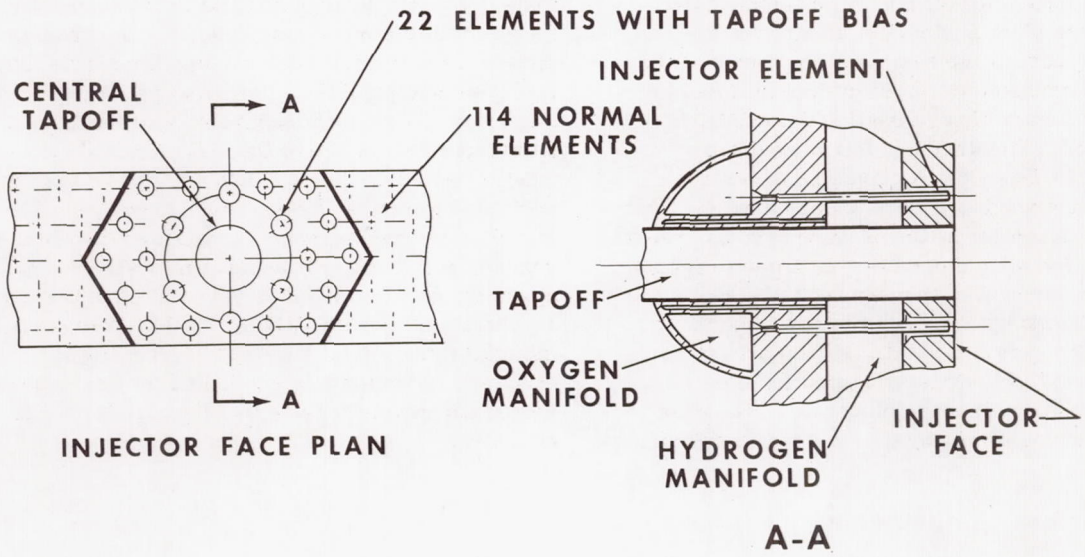

Figure 11. Tapoff injector.

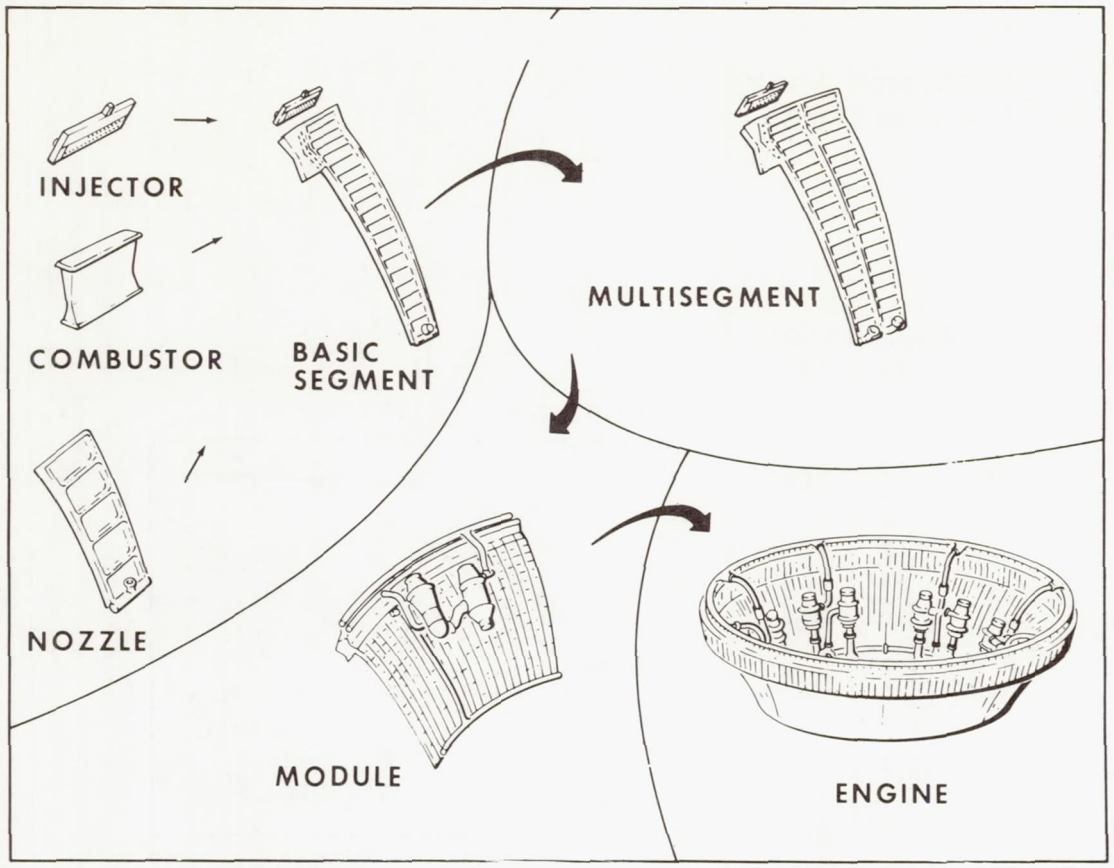

Figure 12. Aerospike building blocks.

chamber, it was possible to optimize the basic design using small, relatively inexpensive hardware. Several segments could then be joined and tested as multi-segments or modules, and finally assembled and tested as a complete engine. In an attempt to minimize the cost of the basic building block of the concept, the combustor, an effort was initiated to determine the feasibility of casting the combustor chamber liner. The design criteria used are summarized in Table 1. An investment casting process summarized in Figure 13 was used for liner fabrication. Machined patterns were used to prepare the waxes which were dipped in a ceramic to form a shell. After removal of the wax from the shell, the copper alloy castings were poured in a vacuum chamber. The ceramic shell was then broken from the casting and the liner was readied for electro-forming the coolant passage closeouts. The case liner at this stage of fabrication is shown in Figure 14.

Completing the cast chamber segment as shown in Figure 15 required electroforming the closeouts and attaching the injector assembly and hydrogen manifolds. The single segment was then readied for test, as shown in Figure 16, by installing the chamber structural members and attaching the nozzle extension. Four complete segments were fabricated in this effort. One of the segments was thoroughly tested in a series of 110 firings. Chamber pressures ranged from 4.14 to 7.72 MN/m^2 (600 to 1120 psia), and mixture ratios varied from 5.6 to 7.9. The remaining three segments were assembled in a multi-segment test configuration shown in Figure 17. This assembly was test fired 22 times at chamber pressures of 2.07 to 8.69 MN/m^2 (300 to 1200 psia) and mixture ratios of 1.5 to 7.6. The post-test hardware condition was good, and the design was judged acceptable for use in a breadboard thrust chamber.

TABLE 1. CAST SEGMENT DESIGN CRITERIA

• Thrust	53.3 kN (12 000 lb)
• Chamber Pressure	8.27 MN/m^2 (1200 psia)
• Mixture Ratio	6.0
• Fuel Inlet Pressure	12.8 MN/m^2 (1850 psia) Maximum[a]
• Oxidizer Inlet Pressure	13.1 MN/m^2 (1900 psia) Maximum[a]
• Cooling Method	Fuel Regenerative
• Chamber Wall Thickness	0.102 to 0.114 cm (0.040 to 0.045 in.)
• Chamber Rib Thickness	0.102 cm (0.040 in.)
• Rib Depth/Rib Width	Up to 3

a. J-25 Turbomachinery Maximum Pressure

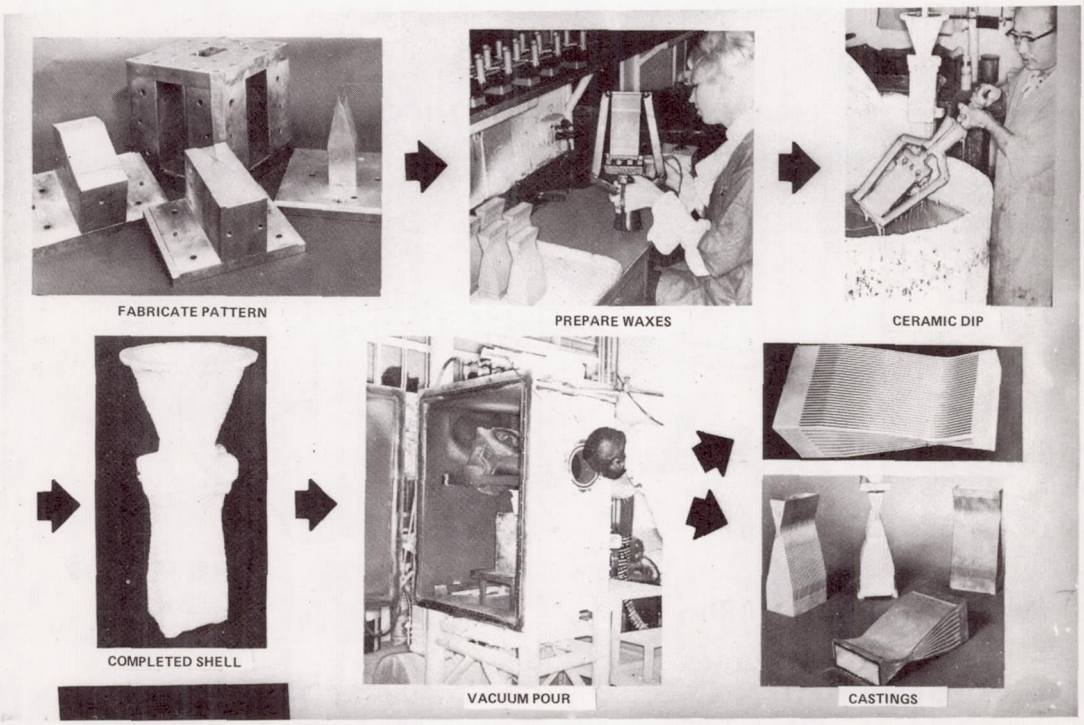

Figure 13. Copper alloy segment — investment casting process.

BREADBOARD THRUST CHAMBER

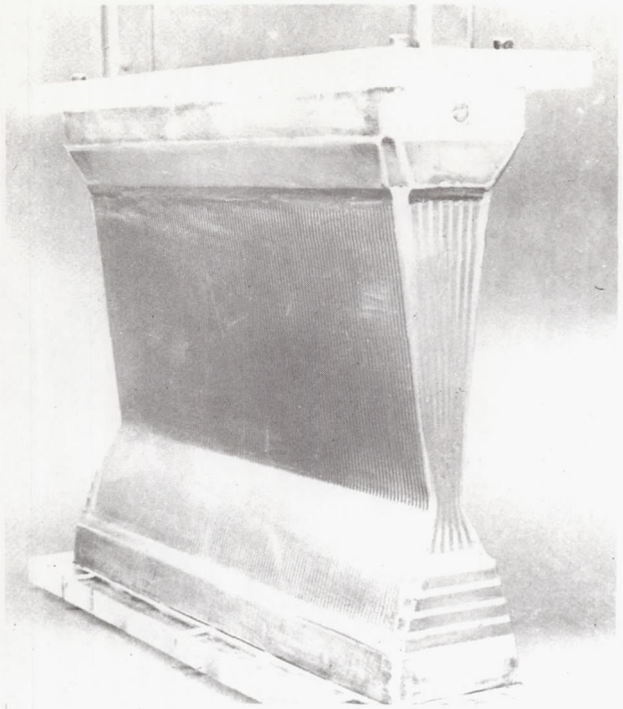

Figure 14. Cast chamber segment.

The breadboard thrust chamber program was initiated to obtain engine system data for an aerospike engine sufficiently large to be representative of a flight system. The selected system, shown in Figure 18, uses 20 of the cast combustion chamber segments developed in the previous segment efforts. A two-dimensional chamber design having 10 segments on each side was selected instead of a round or oval-shaped engine to simplify fabrication and allow the basic segment to be used. J-25 fuel and oxidizer turbopumps are mounted in the center of the engine between the two rows of combustors. Testing of this engine system will provide ignition, transient, and stability data applicable to any future consideration of aerospike engine selection.

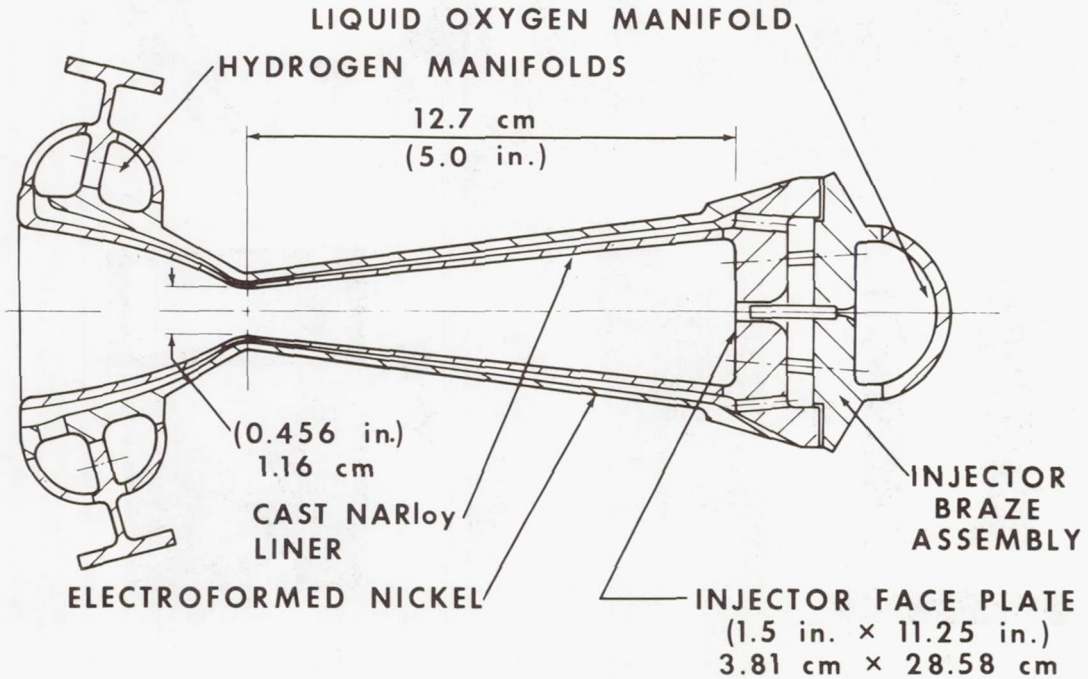

Figure 15. Cast chamber segment.

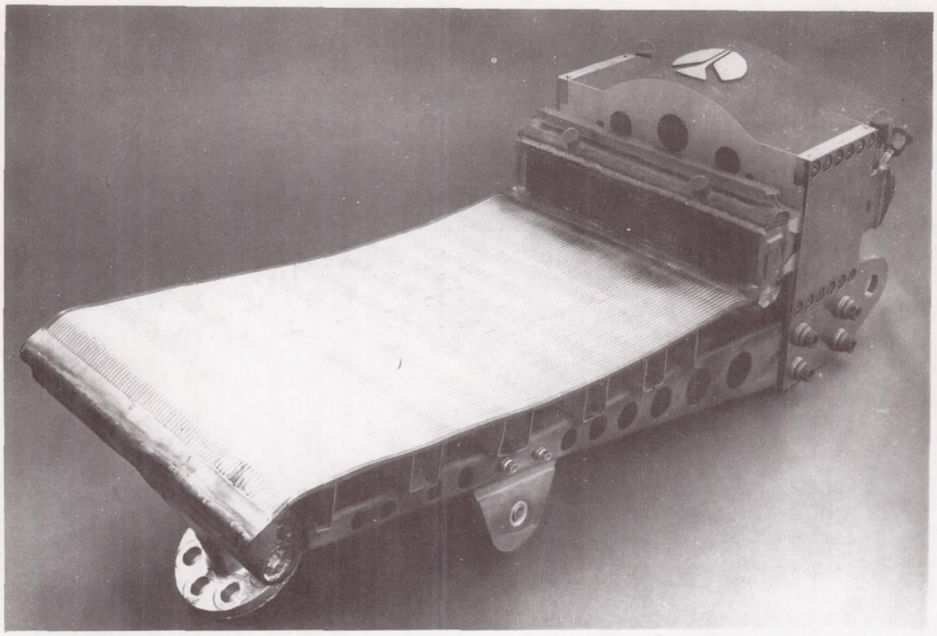

Figure 16. Aerospike single element.

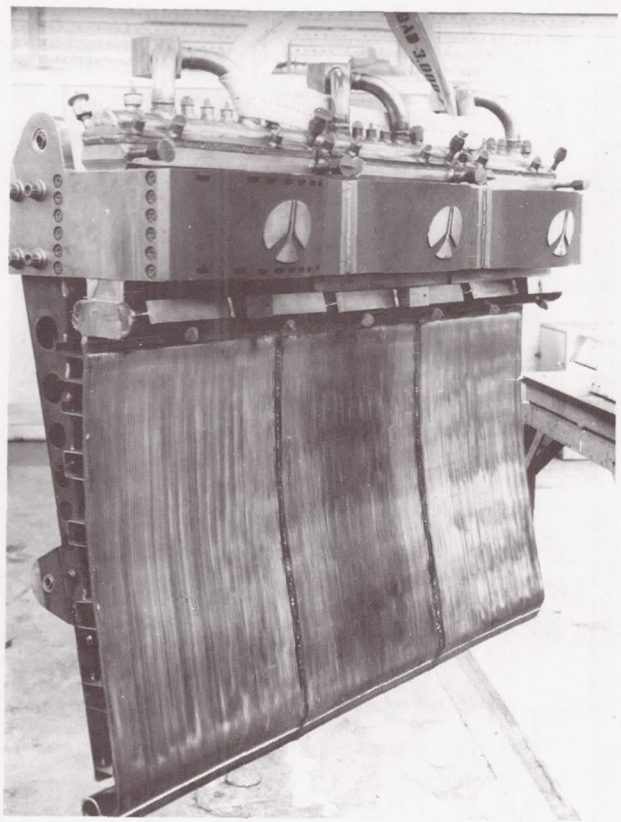

Figure 17. Aerospike multisegment.

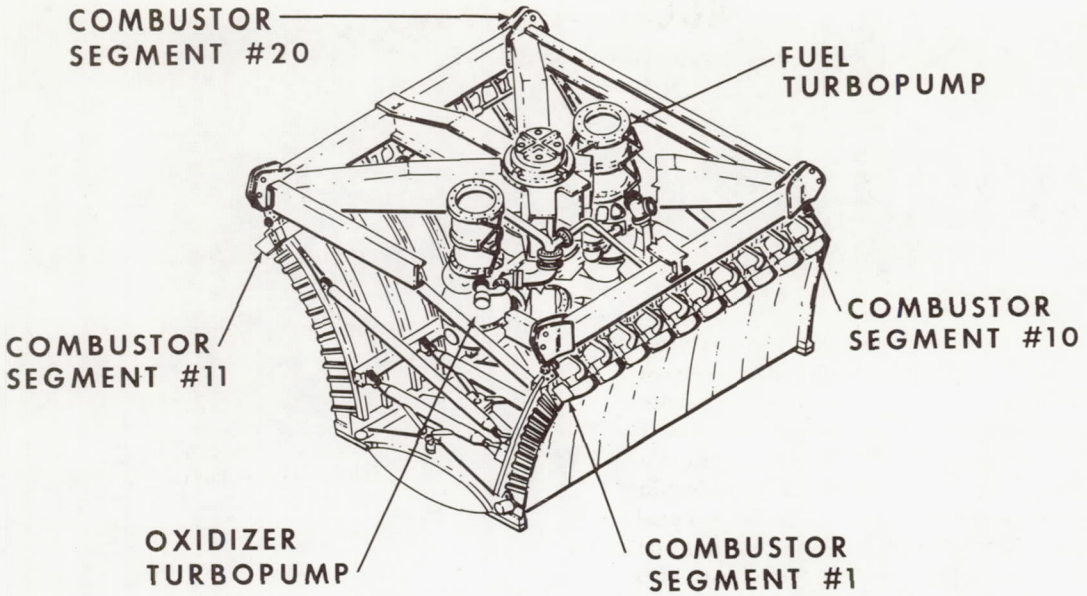

Figure 18. Breadboard thrust chamber.

PERFORMANCE ANALYSIS OF AEROSPIKE ROCKET ENGINES

By

Klaus W. Gross

SUMMARY

The results of an experimental and analytical investigation of the characteristics of the separated flow region for an aerospike nozzle are presented. The primary objective of the investigation was to predict base pressure in the flow recirculation area for open- and closed-wake operation to determine overall engine performance. The developed analytical method and the results of parametric studies including the effects of sonic line shape, internal shock, ambient pressure, base bleed, nozzle area ratio, turbulence effects, plug length, and aerodynamic slipstream are described. A high area ratio, truncated aerospike nozzle as considered by Chrysler Corporation in their single-stage, earth-orbital, reusable vehicle study is discussed, and the performance for various operating conditions is presented.

LIST OF SYMBOLS

Symbol	Definition
A_{ne}	nozzle exit area
A_{nt}	nozzle throat area
C_t	thrust coefficient efficiency
d, j	dividing streamline
L	plug length
L_{max}	ideal plug length
P_{o1}	chamber pressure
P_{amb}	ambient pressure
P_b	base pressure
P_{ne}	nozzle exit pressure
P_{ws}	static-side wall pressure
PR	ratio of ambient and chamber pressure
r	radius normal to nozzle axis
r_3	base radius upstream of recompression shock
r_b	base radius
r_w	trailing wake radius
R, - R	boundary lines separating the mixing free shear layer from the inviscid and base recirculation flow fields
S_L	ordinate of internal shock normal to nozzle centerline
T_{o1}	inviscid flow stagnation temperature
T_b	base flow temperature
u	local velocity in free shear layer
u_a	inviscid flow velocity
x, X	abscissa of coordinate system
y, Y	ordinate of coordinate system
y_m	ordinate of free shear layer
γ	specific heat ratio
ϵ	area ratio

θ	flow angle
$\mathcal{K}$	nondimensional bleed number

INTRODUCTION

In the past, primarily classical rocket engines of the bell type have been used for the propulsion of launch and space vehicles. In the future, advanced rocket propulsion systems will require exhaust nozzles that perform efficiently over a wide range of ambient operating conditions. Furthermore, these exhaust nozzles should be short, lightweight, and relatively easy to cool. Analyses and tests have demonstrated that a group of nozzles referred to as altitude compensating nozzles satisfy these requirements. The expansion-deflection and aerospike nozzles are included in this group (Fig. 1). Altitude compensation in these nozzles is obtained by the flow of the combustion products in the supersonic range. Unlike the bell nozzle, in which the entire flow is contained within a fixed contour, the flow of an aerospike nozzle is guided along the plug only. The outer shroud ends shortly after the nozzle throat and forces the flow to establish its own external contour which must be in pressure balance with the ambient condition. This document will discuss only those aspects relating to the performance analysis of the aerospike nozzle.

AEROSPIKE ENGINE PERFORMANCE

The performance of an aerospike nozzle is composed of two portions; namely, thrust produced by pressure forces acting on (1) the solid wall surfaces guiding the flow and (2) the base area. The latter item primarily will be discussed in this report since it affects performance significantly.

OPEN-CLOSED WAKE OPERATION

Dependent on the chamber-to-ambient-pressure ratio, two significant nozzle operation modes can be identified. At a low pressure ratio, the separated base flow region is open and is sensitive to ambient conditions through the trailing wake corridor. For a high pressure ratio, the base flow field becomes closed preventing any influence of the ambient environment. Experiments have shown that during the open-wake condition the base pressure varies in accordance with the ambient pressure. After the

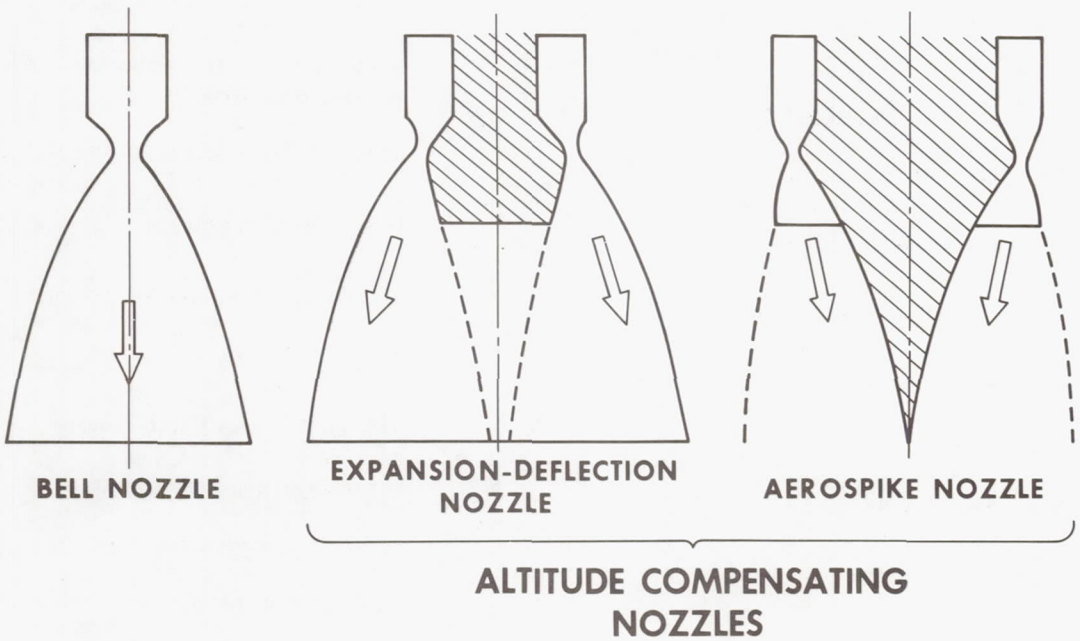

Figure 1. Nozzle types.

wake closes, the base pressure remains constant (Fig. 2).

ANALYTICAL FLOW TREATMENT

The total flow field beginning at the injector can be subdivided into the realms where viscous forces are either negligible or dominant. Viscous effects are insignificant in the core portion of the subsonic, transonic, and supersonic flow fields; whereas strong viscous effects, generated by the interaction of the core flow with the ambient environment and the base recirculation region, must be considered in the boundary layer along the solid surfaces and in the free shear layers (Fig. 3). However, there exist phenomena caused by the boundary and free shear layer which affect the inviscid flow field significantly. Because of the viscous behavior, the boundary layers do not separate from the wall contour at the end of the outer shroud and plug truncation corner, rather they bend around these wall discontinuities and then separate. This effect produces a local overexpansion of the inviscid core flow, represented by an expansion fan. Afterwards, the flow balances itself by changing direction resulting in the generation of internal, lip, and recompression shocks (Fig. 4).

After determination of the chamber and nozzle geometry, the theoretical analysis of the inviscid flow field begins with the calculation of the combustion reaction in the chamber based upon propellant combination, chamber pressure, and mixture ratio. The results are used in a transonic model to generate a sonic start line that, in turn, will be used to calculate the supersonic flow field by the rotational method of characteristics. Solutions of the free jet boundary, internal shock, and recompression shock are included.

The performance of the nozzle down to the plug truncation corner is then determined from the inviscid flow analysis reduced by the losses from the boundary layer. The performance contribution from the base pressure depends upon whether an open- or closed-wake condition exists. For

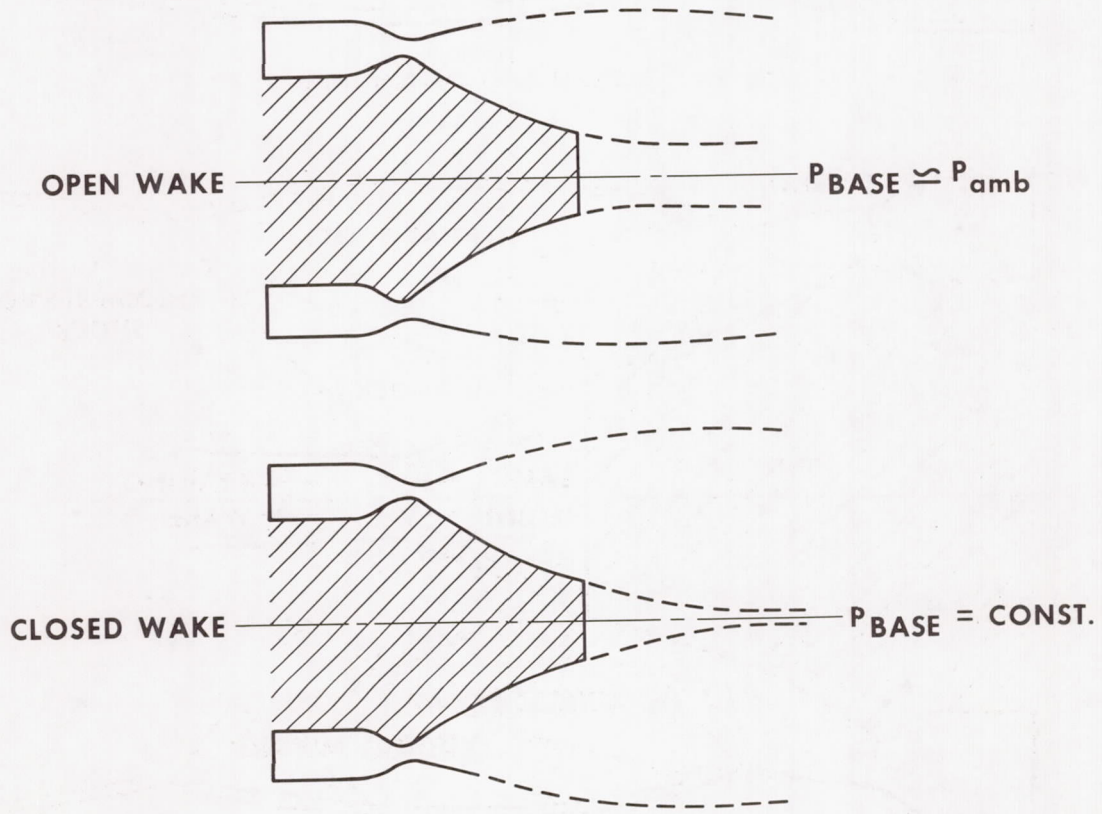

Figure 2. Truncated plug nozzle operation mode.

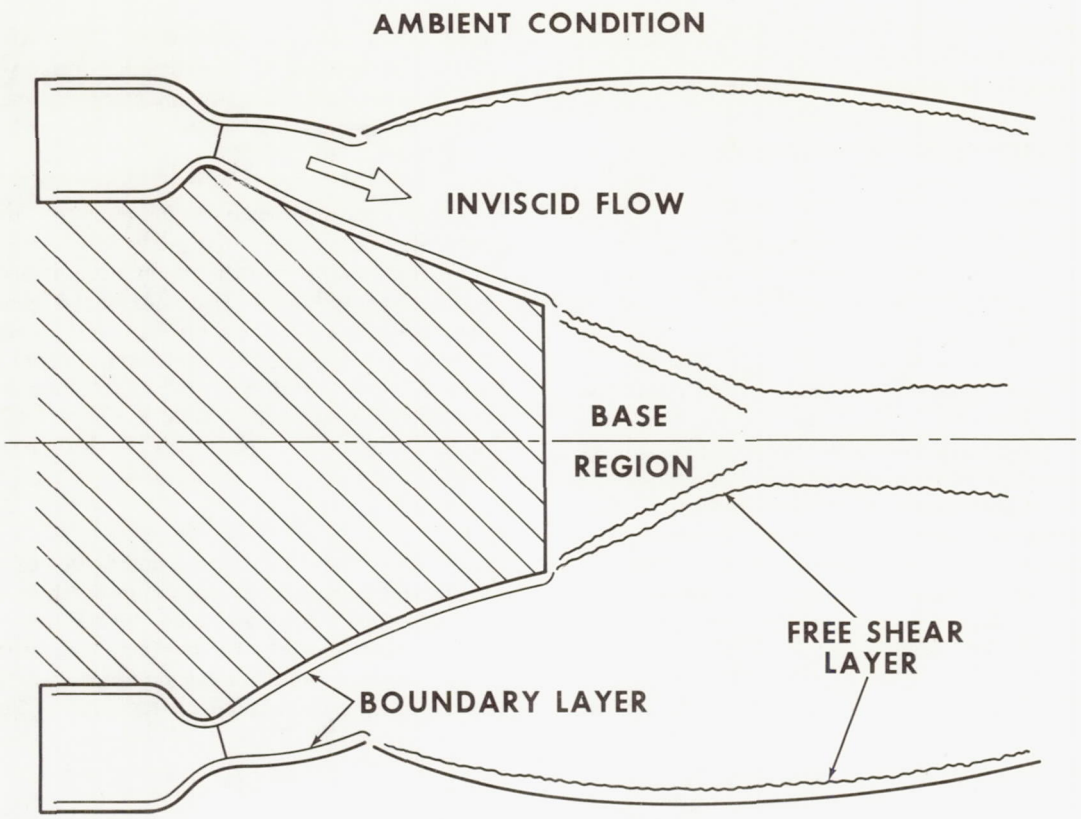

Figure 3. Analytical flow field treatment.

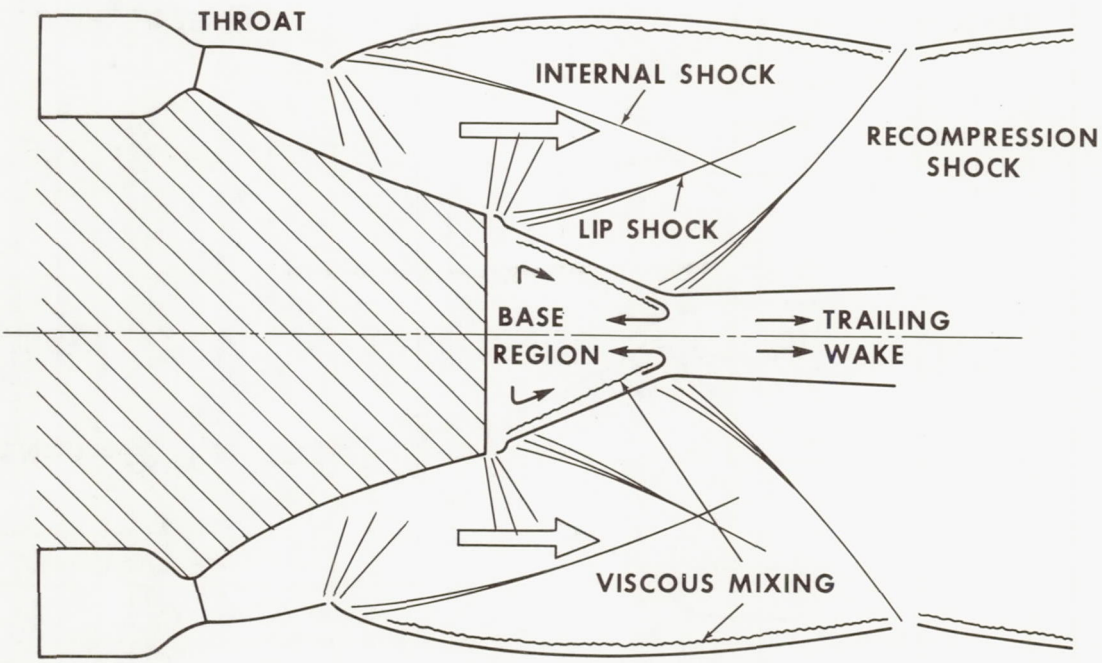

Figure 4. Plug nozzle flow field (closed wake).

open-wake flow the base pressure is slightly lower than the ambient pressure and is approximately constant across the whole base area. Under a closed-wake condition, the base pressure is determined as discussed in the following (Fig. 5).

Downstream of the plug corner a domain, bordered by the lines R and -R, exists in which the mixing free shear layer develops. Within this domain lies one streamline that separates the base recirculation flow from the remainder of the flow field. From the previous analysis the flow conditions just upstream of the corner at location (1) are known. Now, an assumption of the base pressure P_b is made. This base pressure value is assumed to exist at location (2), since a pressure gradient across the shear layer is very small. With the two known pressures, a Prandtl-Meyer expansion can be performed, resulting in the flow angle θ_{1-2} reflecting a conical surface. This cone serves as a geometrical boundary condition and allows one to proceed with the method of characteristics calculation until the trailing wake radius r_w is reached. Simultaneously, the flow condition at location (3) is specified. At this point the flow outside the recirculation area is turned in an axial direction by an angle θ_{3-4}, which is equal to θ_{1-2}, and this results in the generation of a recompression shock. Application of the method of characteristics simulates this occurrence and leads to the flow condition at location (4). Within the shear layer dynamic energy is lost because of the viscous effects, thereby lowering the total pressure continuously. For the correct base pressure solution, the following criterion must be satisfied: the static pressure at location (4) is equal to the total pressure of the streamline dividing the recirculation base flow from the external flow. This means that all particles within the recirculation flow field have a lower total pressure and cannot flow further downstream but will be recirculated instead. If the criterion at the wake radius location is not satisfied, a new base pressure P_b must be assumed and the calculation must be repeated until convergence is obtained.

At present a theory does not exist that determines the location of the recompression shock. Therefore, an empirical relationship relating the wake radius to the Mach number of the inviscid flow at location (1)

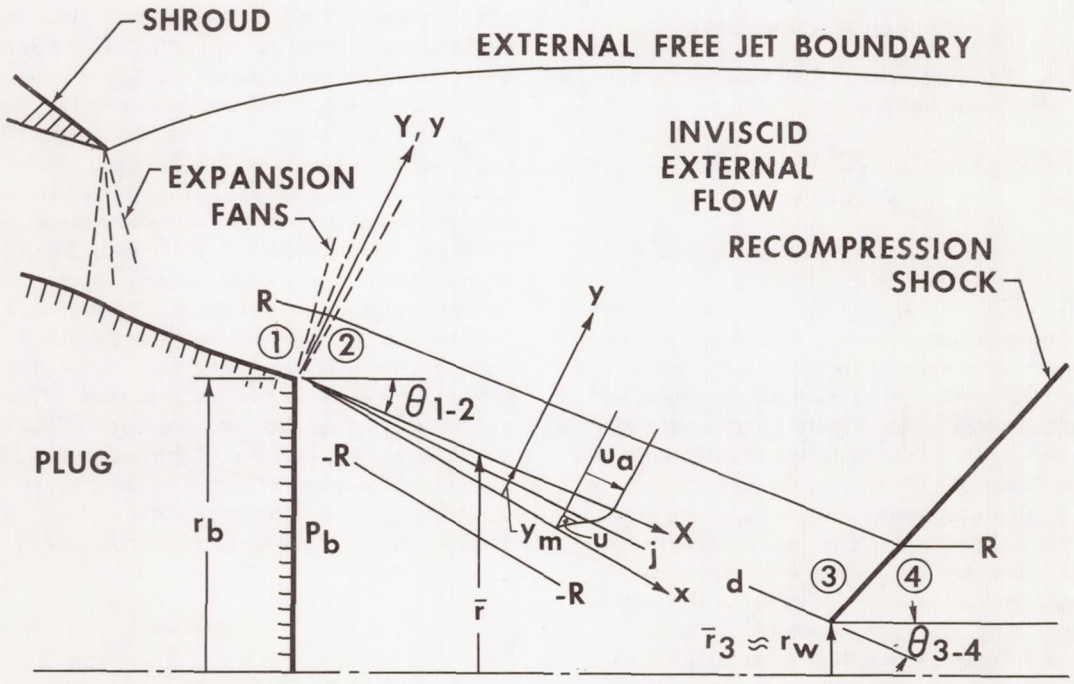

Figure 5. Flow model for the determination of the turbulent base pressure for an axisymmetric plug nozzle.

has been generated (Fig. 6). From this graph a wake radius is obtained for a given approach Mach number, and it is used in the base pressure solution procedure.

It should be mentioned that a base pressure solution for an expansion-deflection nozzle is determined by the same analogy.

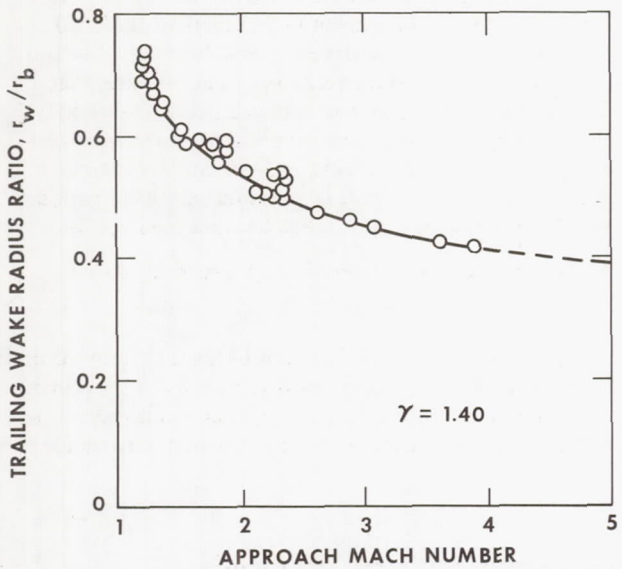

Figure 6. Trailing wake radius ratio versus Mach number for $\gamma = 1.40$

PARAMETERS AFFECTING NOZZLE PERFORMANCE

Sonic Line Shape

For the analytical solution, it is important to know the correct shape and location of the sonic line. Since the method of characteristics solution is based upon a start line slightly greater than Mach number equal to one, it is apparent that the complete supersonic flow field and the nozzle performance is governed by this parameter. Because of the aerospike nozzle geometry, the physical nozzle throat area is not normal to the engine centerline but is inclined by a specific angle. Because of the nozzle contour geometry, the combustion products are accelerated differently such that an axisymmetric sonic line shape, even with regard to the nozzle throat centerline, is not formed. In Figure 7 measurement location, static pressures converted to Mach number, and the interpolated sonic line are presented. To obtain the effect of various sonic line shapes on the base pressure, four different start lines symmetric to the geometric throat were selected. The analytical results presented in Figure 8 indicate that the closed recirculation area and the location of the recompression shock do not change. The base pressure, however, is affected by the start line profile.

Ambient Pressure

In Figure 9 the flow fields of a planar truncated plug nozzle for various ambient-to-chamber-pressure ratios are presented covering the open- and closed-wake operation mode. The respective base pressure measurements, nondimensionalized by the chamber pressure, are shown in Figure 10 as a function of the external or ambient pressure. During open-wake operation [Figs. 9(a), 9(b), 9(c), and 9(d)], the base pressure follows the ambient pressure very closely. As soon as the closed-wake condition is reached [Figs. 9(e) and 9(f)], the base pressure remains constant.

In contrast to the planar nozzle, Schlieren photographs of an axisymmetric truncated plug nozzle for various ambient pressures are shown in Figure 11 with corresponding base pressure measurements presented in Figure 12. In principle the same characteristics occur in both flow field pictures; however, for the three-dimensional case the characteristics seem to be more pronounced. Here again the base pressure follows the ambient pressure closely [Figs. 11(a) and 11(b)] during the open-wake condition. However, lowering the ambient pressure from the condition shown in Figure 11(b) to that shown in Figure 11(c) generates a sudden increase in the base pressure. This pressure rise is caused by the internal shock emanating from the outer shroud striking the surface of the plug. A further reduction in ambient pressure [Figs. 11(c) and 11(d)] makes the base pressure follow the same trend, however, because of the presence of the internal shock at an elevated pressure level. Finally, when the recirculation wake closes [Figs. 11(e) and 11(f)], the base pressure remains constant.

Base Bleed

Introduction of base bleed flow into the base recirculation area may be used to increase the base pressure and consequently raises the nozzle

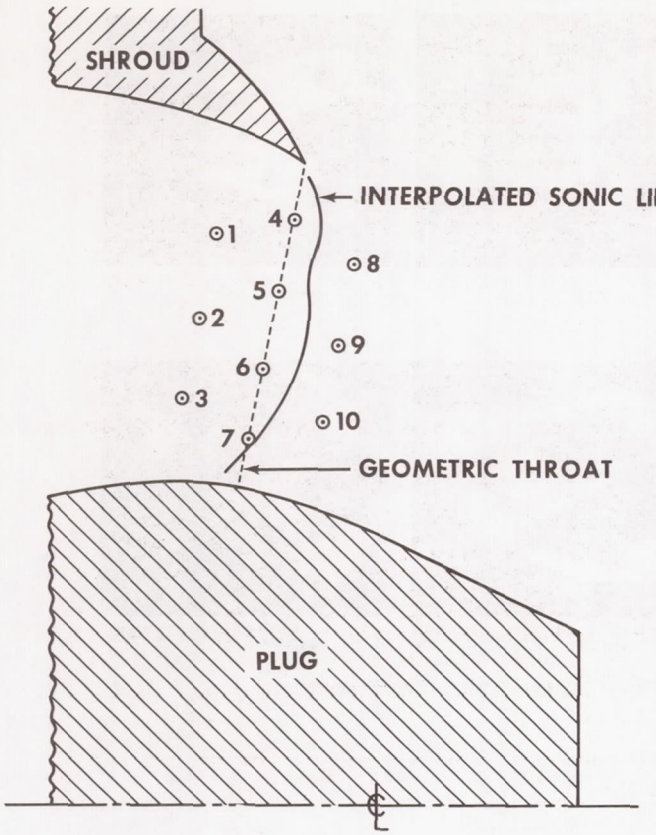

PRESSURE TAP	MACH NO.
1	0.66
2	0.72
3	0.81
4	0.88
5	0.90
6	0.91
7	0.99
8	1.18
9	1.10
10	1.12

Figure 7. Location of interpolated sonic line with respect to geometric throat.

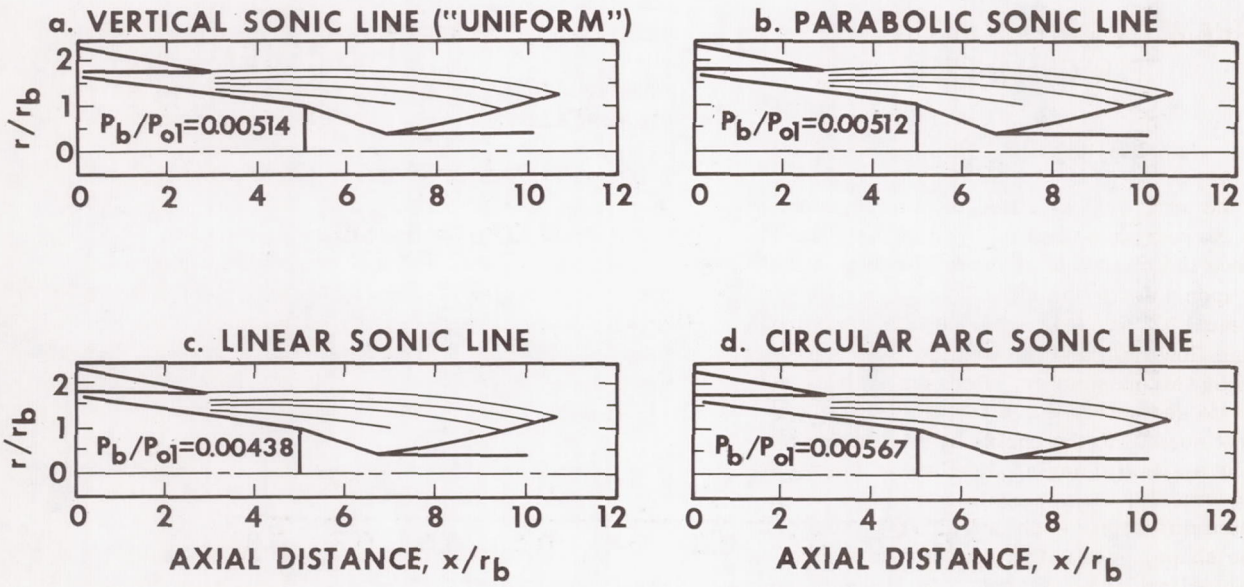

Figure 8. The influence of sonic line shapes for an axisymmetric internal-external-expansion truncated plug nozzle.

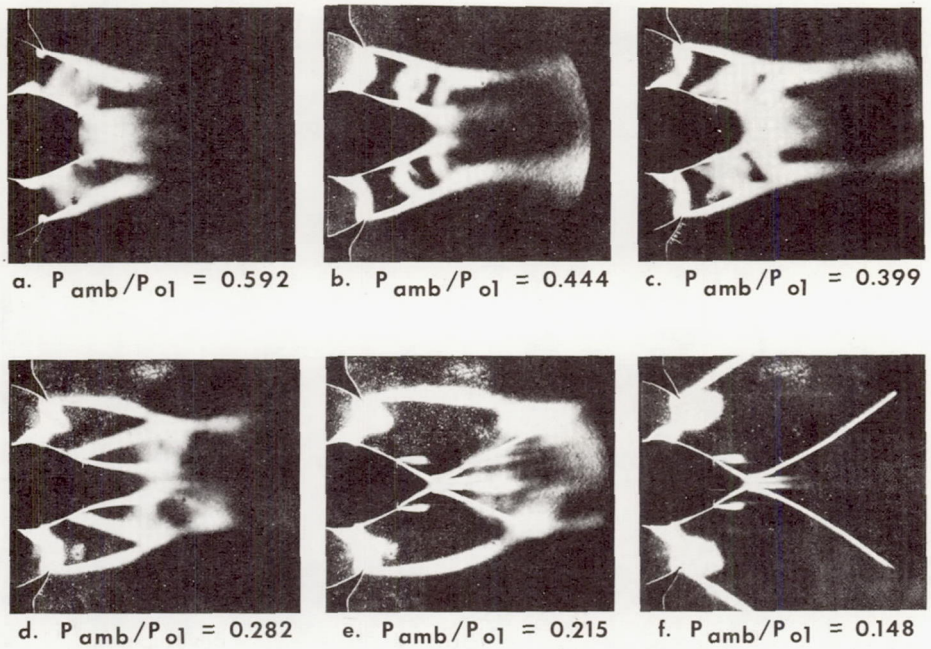

Figure 9. Truncated plug nozzle flow development.

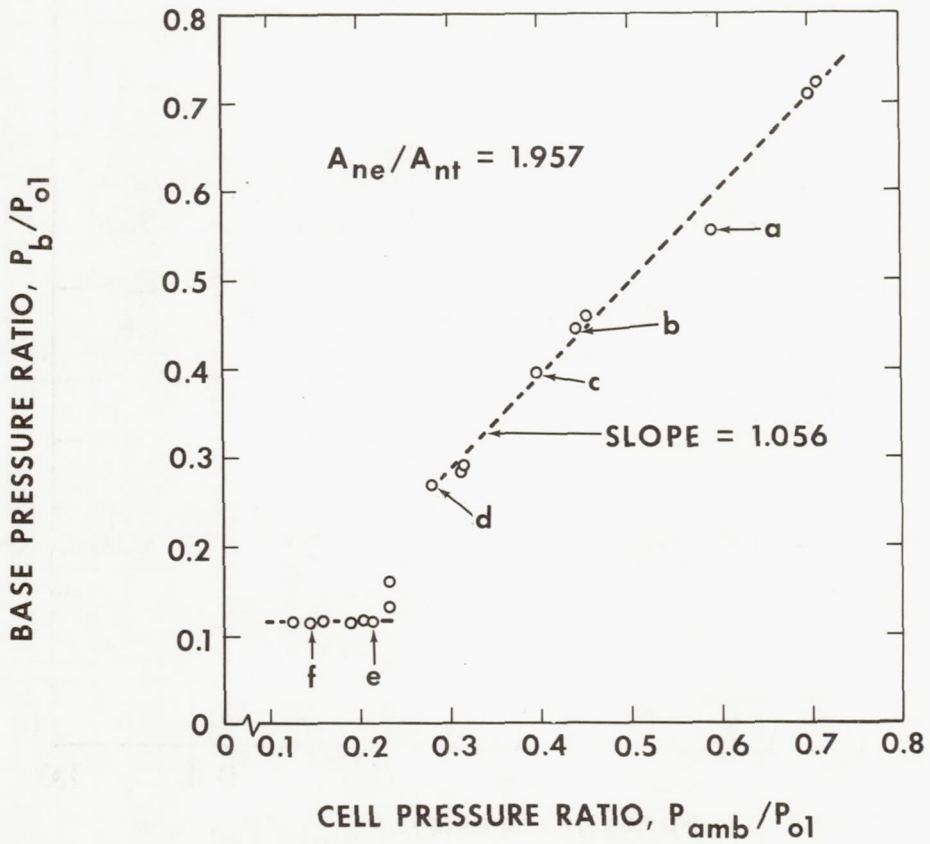

Figure 10. Variation of planar truncated plug nozzle base pressure ratio with ambient pressure ratio.

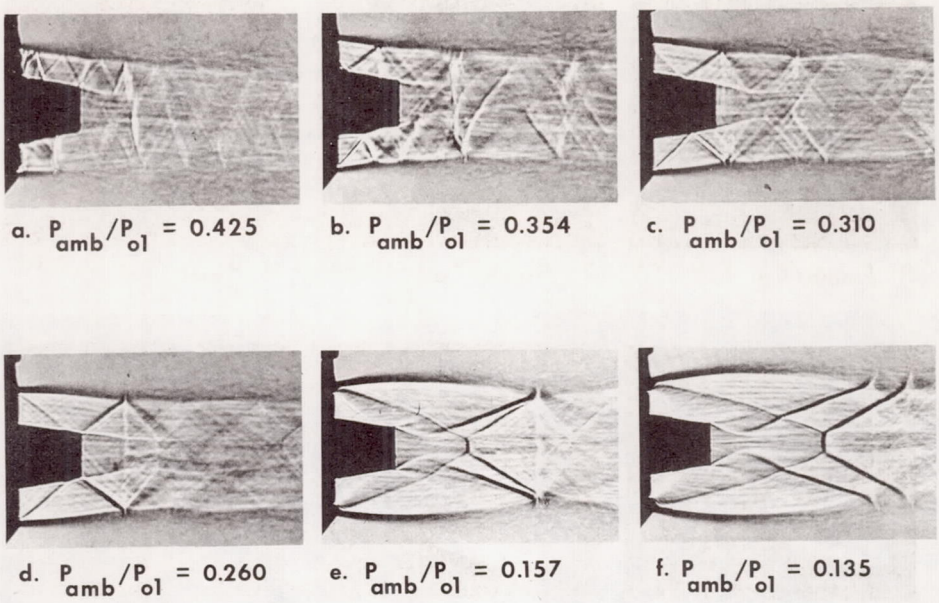

Figure 11. Axisymmetric truncated plug nozzle flow development.

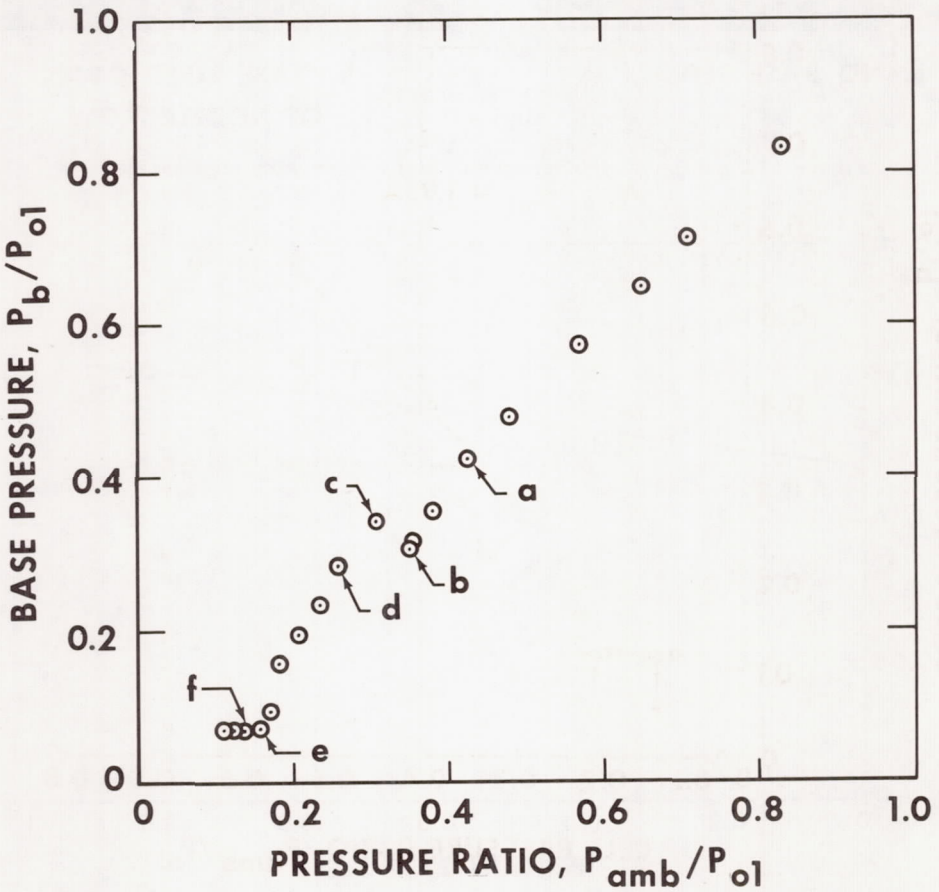

Figure 12. Axisymmetric truncated plug nozzle operating characteristics.

performance. Also, it could be used as a possible means of cooling the plug. Figure 13 shows Schlieren photographs for a test configuration with 0-percent and approximately 1-percent base bleed flow. It is evident from these photographs that even a small bleed rate produces a marked change in the visual flow pattern. The neck of the wake is noticeably thicker and the wake length appears to be longer. Also, the lip shock, which is barely visible in the no-bleed case, has become clearly defined in the flow field with bleed and has changed its position. The effect of base bleed on the nozzle base pressure is presented in Figure 14. As expected, the base pressure increases linearly with base bleed. At approximately 1-percent base bleed with regard to the total flow, a base pressure ratio increase of 30 percent is possible. For base bleed flow greater than 1 percent, the base pressure rise becomes very small and the concept loses its effectiveness. In case of performance optimization, a base bleed flow

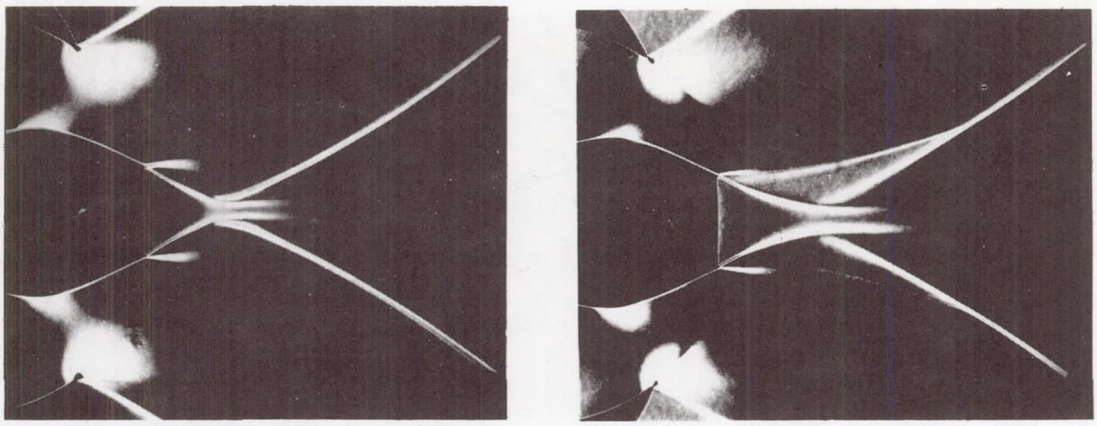

Figure 13. Schlieren photographs of planar truncated plug nozzle.

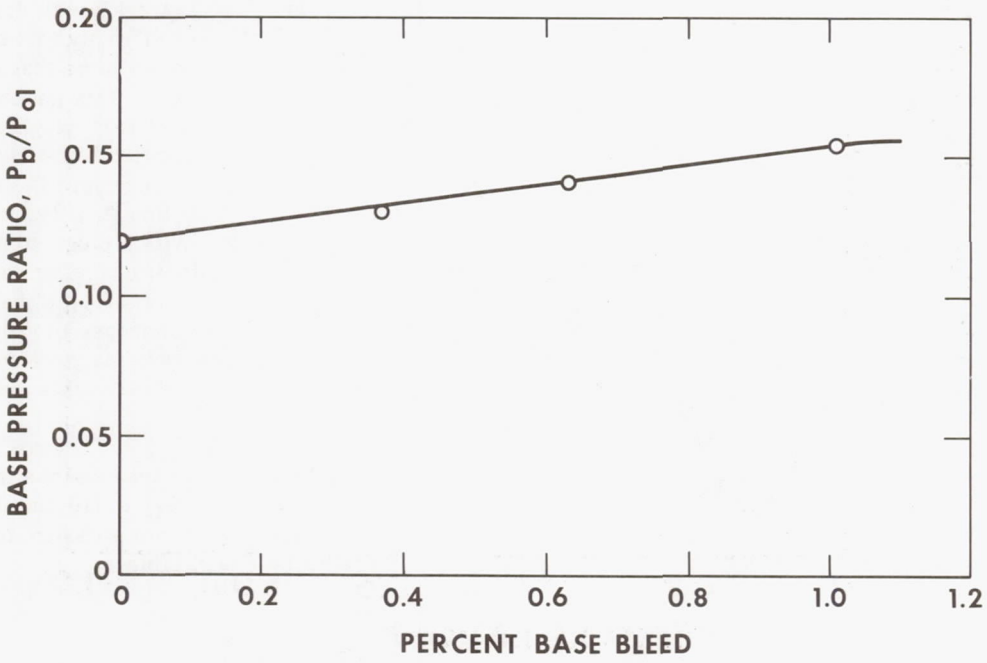

Figure 14. Effect of base bleed on base pressure of truncated plug nozzle.

must be selected such that divergence of this flow from the main chamber flow does not deteriorate the chamber performance significantly, and although the base pressure has been increased, the overall performance is lower.

Nozzle Area Ratio

Increasing the velocity of the combustion products and, therefore, the thrust is possible by varying the overall area ratio A_{ne}/A_{nt} of the nozzle. Results of an analytical investigation are exhibited in Figure 15. Note that an increasing area ratio produces a corresponding decrease in the base pressure. This result is to be expected, since an increasing overall area ratio implies a higher design Mach number of a nozzle.

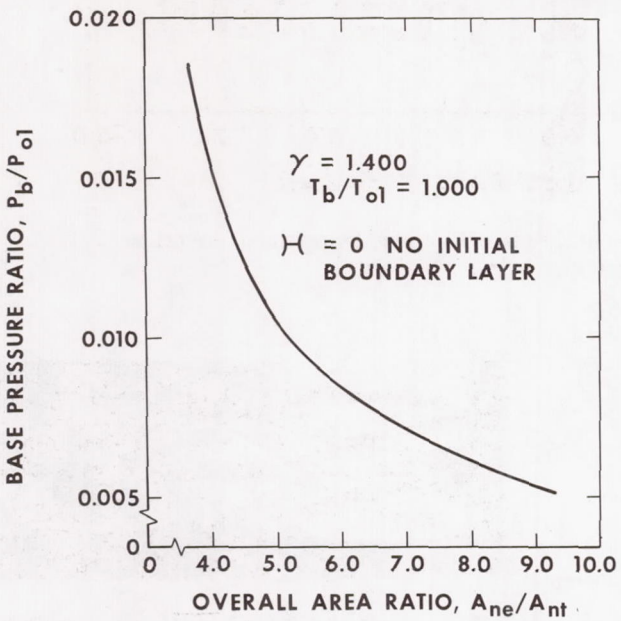

Figure 15. Influence of area ratio on the base pressure ratio of an axisymmetric internal-external-expansion truncated plug nozzle.

Turbulence Effects

Laminar or turbulent flow, especially in the boundary layer, significantly affects the location of the flow where transition from a subsonic to a supersonic condition occurs. The nozzle test configuration, as analytically designed, indicated λ shocks upstream of the geometric throat. Boundary layer trips installed in the subsonic flow area reduced the sequence of λ shocks to a single strong shock which appeared as a slightly curved normal shock. This observation revealed that under normal operating conditions, the boundary layer was laminar and that with the trip, the boundary layer became turbulent. Translating the plug physically downstream by a small amount eliminated the shock formation in the nozzle convergent area. At the same time the effects of turbulence on the nozzle centerline static pressure distribution and the base pressure were investigated. In addition to the boundary layer trip a 0.64-cm (0.25-in.) wire mesh was installed at the inlet to the nozzle section to induce turbulence in the entire flow field. The resulting measurements are shown in Figure 16. The largest deviation in the base recirculation area [from 0 to 2.54 cm (0 to 1.0 in.) distance from the plug base] occurred with the wire mesh and was on the order of 8 percent. The boundary layer trip does not appear to have affected the static pressure distribution in this area. Variation in the base pressure demonstrated the same trends.

Plug Length

In general it is desirable to have as high a closed-wake base pressure as possible to obtain the maximum thrust. Experimental results obtained for the same nozzle configuration with varying plug lengths (Figs. 17 and 18) imply that the most desirable configuration would be that with the plug ending at the shroud exit. This geometry also has the obvious advantages of less weight and a shorter length. However, since the thrust contribution resulting from the base pressure is usually not the major part of the total thrust, other considerations are also important. With a plug extending beyond the shroud exit, the additional plug surface may gather enough thrust to offset both the decrease in base pressure and the increase in weight. Although the base pressure tends to increase for plug lengths greater than $L/L_{max} \approx 0.5$, this extreme of plug length is not practical. As L/L_{max} approaches 1.0, both the plug base area and the increase in plug surface area become very small and the changes in total thrust resulting from pressure forces on these surfaces become negligible.

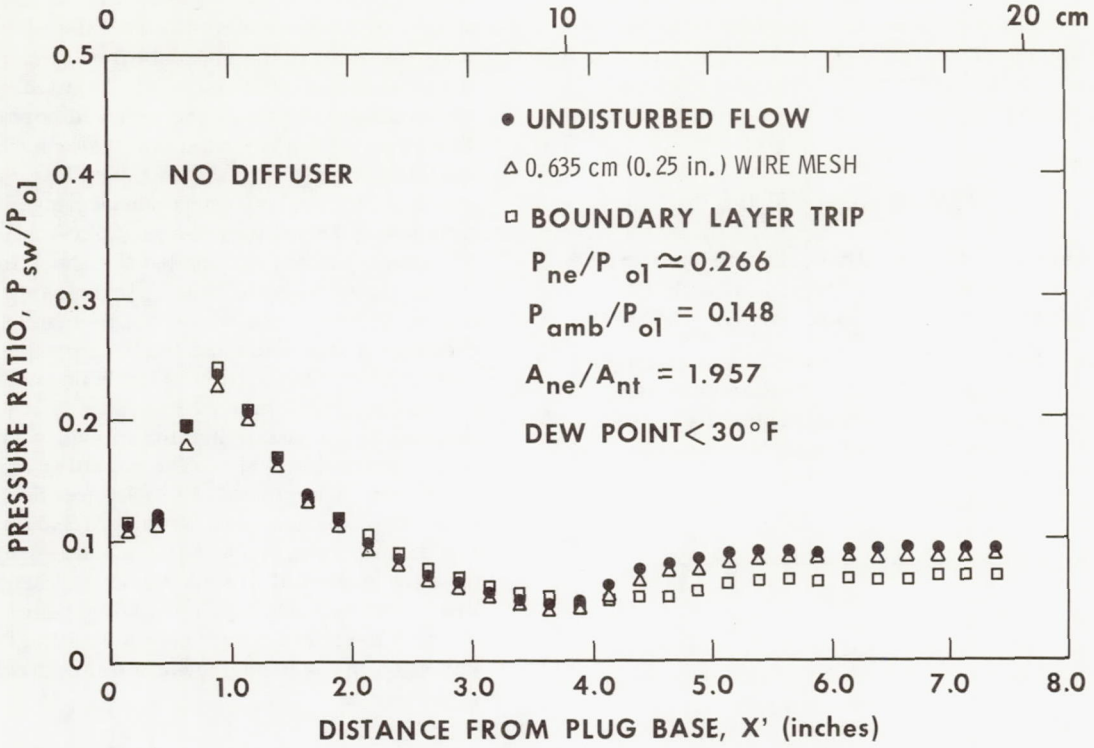

Figure 16. Induced turbulence effects on side-wall centerline static pressure variation of planar truncated plug nozzle.

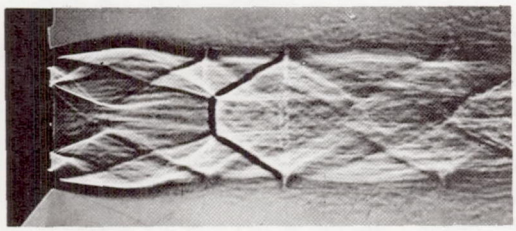

a. $P_{amb}/P_{ol} = 0.135; L/L_{max} = 0.218$

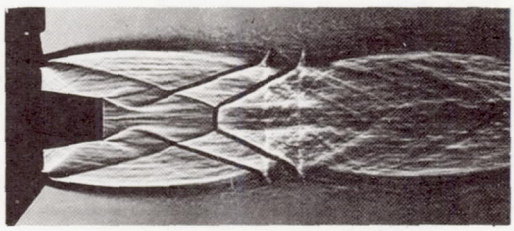

b. $P_{amb}/P_{ol} = 0.135; L/L_{max} = 0.481$

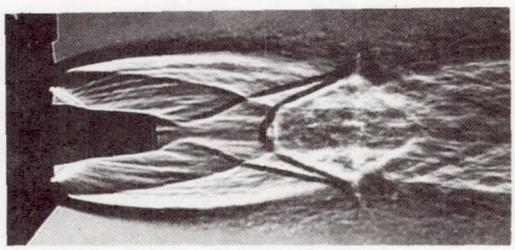

c. $P_{amb}/P_{ol} = 0.104; L/L_{max} = 0.641$

Figure 17. Nozzle flow fields for three different plug lengths.

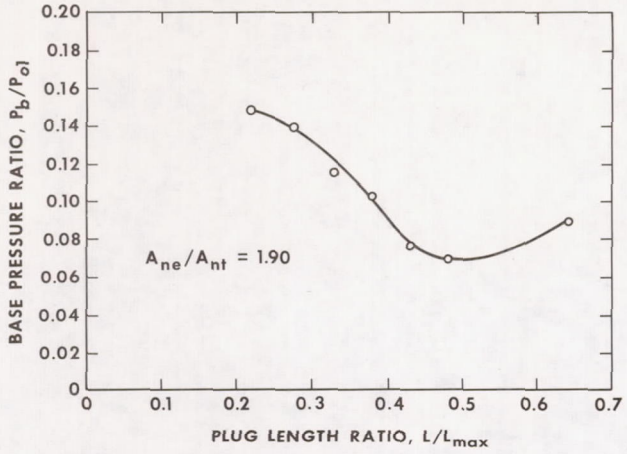

Figure 18. Effect of plug length ratio on the closed-wake base pressure for axisymmetric truncated plug nozzle.

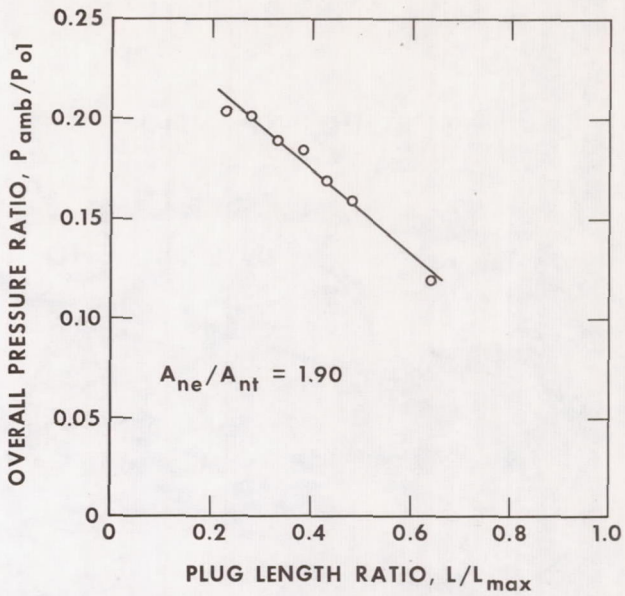

Figure 19. Effect of plug length ratio on overall pressure ratio at wake closure for axisymmetric truncated plug nozzle.

The overall pressure ratio at which the wake closes is important for determining optimum nozzle efficiency. Figure 19 presents this relationship. The increase in overall pressure ratio at wake closure as the plug length ratio is decreased presents further justification for the desirability of shorter plugs. The calculation of total performance for a given mission is greatly facilitated if the base pressure is constant (closed wake) for the longest period possible. Figure 19 indicates that shorter plug lengths lead to the establishment of closed-wake operation at higher values of ambient pressure, i.e., lower altitudes, and therefore increase the percentage of vehicle flying time at the closed-wake condition.

Experimental-Analytical Flow Field Comparison

A flow field Schlieren photograph of an axisymmetric truncated plug nozzle is shown in Figure 20. For performance determination, the subsonic and transonic flow field is of vital importance. However, in the supersonic area, only the flow field bounded by the shroud surface, plug surface, free jet boundary, separated base flow region down to the location of the recompression shock location, and the recompression shock itself is significant.

A comparison between the observed free jet boundary and internal shock location with analytical predictions is presented in Figures 21 and 22. The predicted constant pressure boundary deviates slightly from the observed location downstream of the outer shroud; this deviation was caused by the assumption of flow overexpansion around the shroud lip. In the case of the internal shock location, again a small difference occurs that results from the flow overexpansion assumption and also from the selected shape of the start line governing the supersonic flow field calculation. More accurate input data for the analytical concepts would eliminate these differences.

In Figure 23 the analytical results are superimposed on the Schlieren photograph. In addition to the previously mentioned parameters, the base recirculation area shape, the trailing wake shape, and the recompression shock shape are shown, and they agree well with the observed highly complicated flow field.

Aerodynamic Slipstream

The Chrysler Corporation, Space Division, recently investigated the performance of an aerospike engine in a feasibility study of a single-stage, earth-orbital, reusable vehicle (SERV). The engine is integrated into the base area of the cone-shaped vehicle (Fig. 24). Because of the enormous base area of the aerospike engine, which contributes greatly to the overall propulsion, the performance

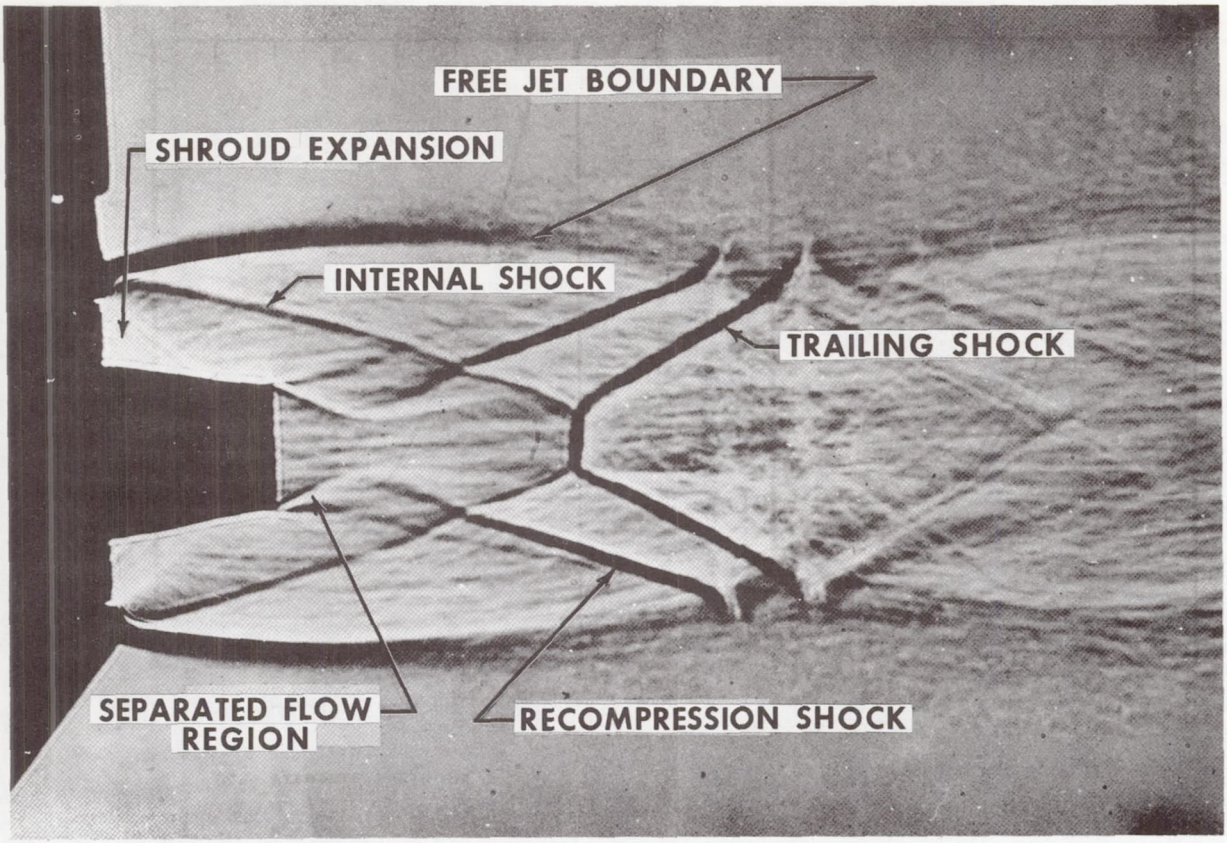

Figure 20. Flow field of the axisymmetric internal-external-expansion nozzle.

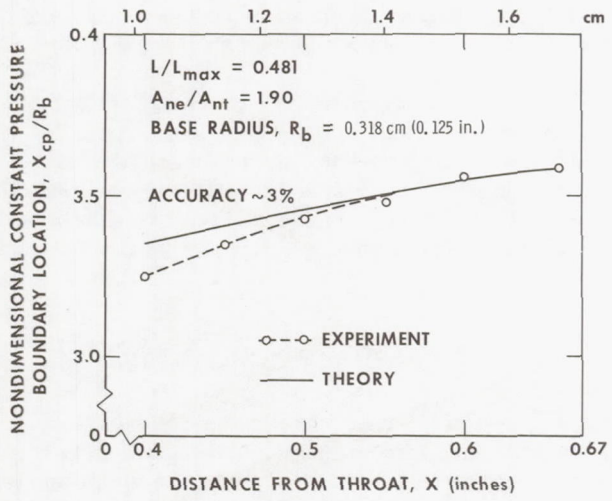

Figure 21. Comparison between analytical and observed constant pressure boundary location for axisymmetric truncated plug nozzle.

during open-wake operation and the condition of wake closure was important. When the vehicle flies through the atmosphere, the body geometry produces a slipstream with conditions in the aerospike engine area that are different from the undisturbed environment. The free jet boundary formed between the nozzle exhaust flow and the ambient air will adapt to the local condition and therefore affect the inviscid nozzle flow field, the base recirculation area, and the base pressure. Since most aerospike nozzle testing has been performed in still air, a wind tunnel test program with a 2.5-percent scaled SERV model using air flowing through the engine was executed to investigate the slipstream or Mach number effect on performance. The results of the test data, modified by scaling laws to account for the full size geometry and hot engine firing, are presented in a so-called carpet plot in Figure 25. This carpet plot does not show any numbers on the abscissa and has been generated by using equal intervals between each 3048-m (10 000-ft) interval for the zero Mach number condition. Such a plot is very convenient for data

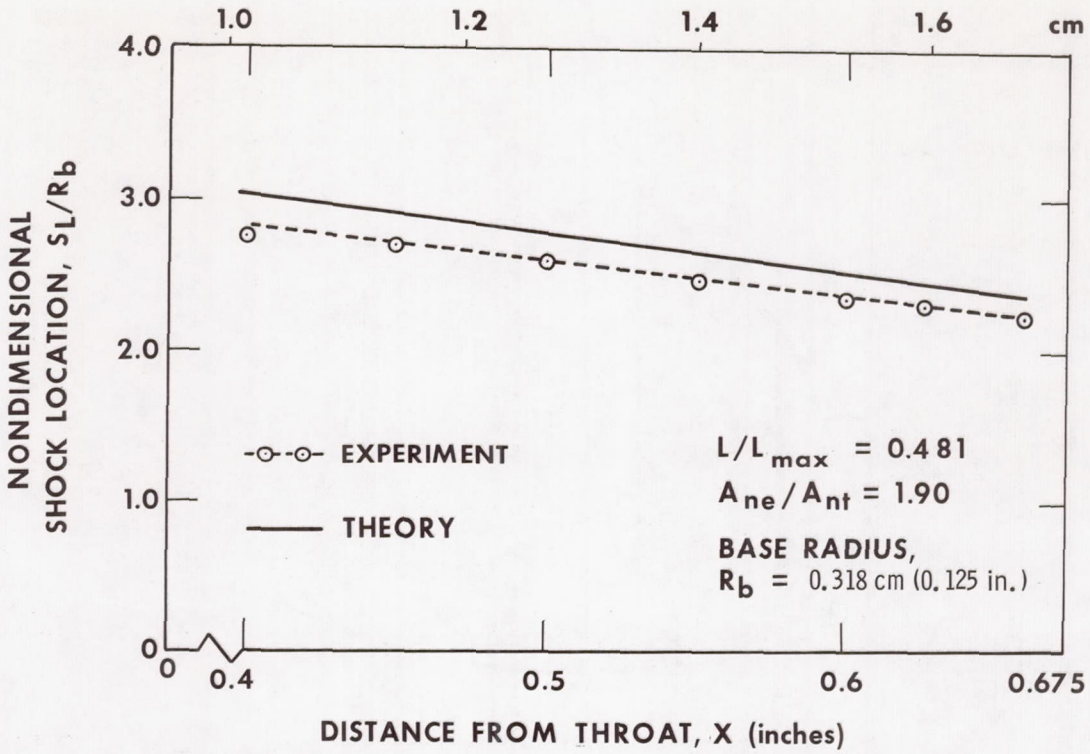

Figure 22. Comparison between analytical and observed internal shock location for axisymmetric truncated plug nozzle.

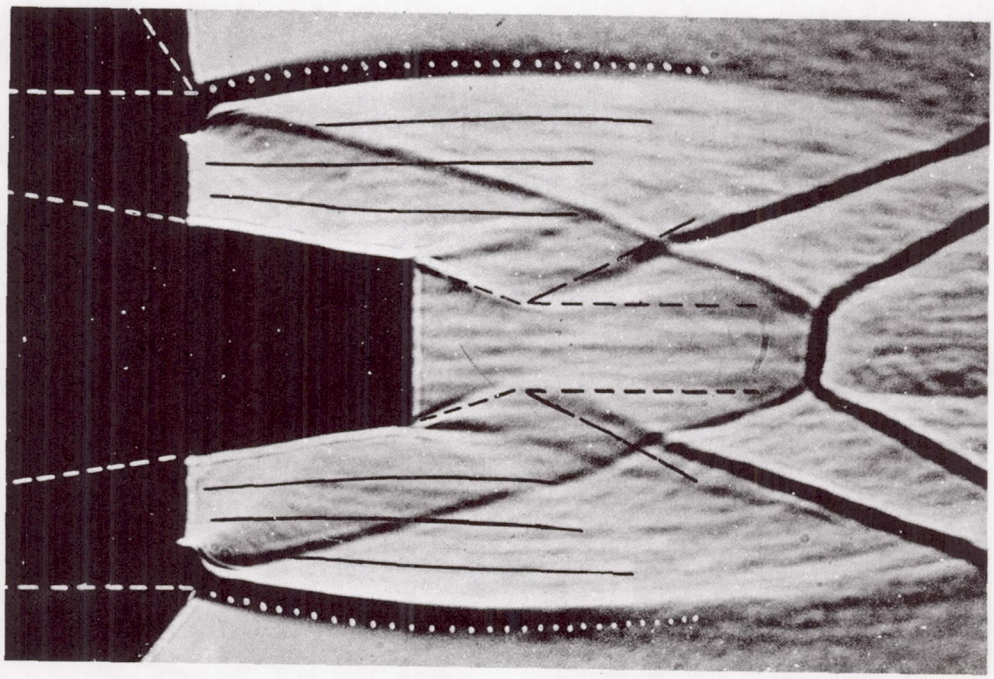

Figure 23. Experimental and analytical comparison of the flow fields of an axisymmetric internal-external-expansion nozzle.

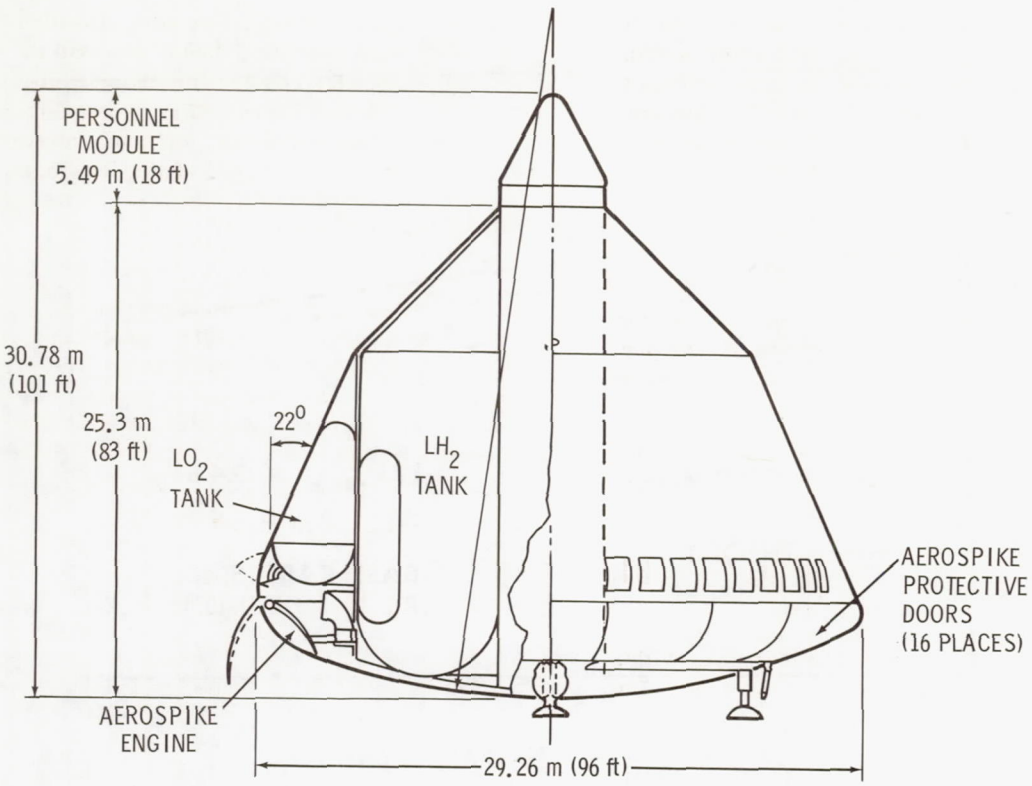

Figure 24. SERV vehicle.

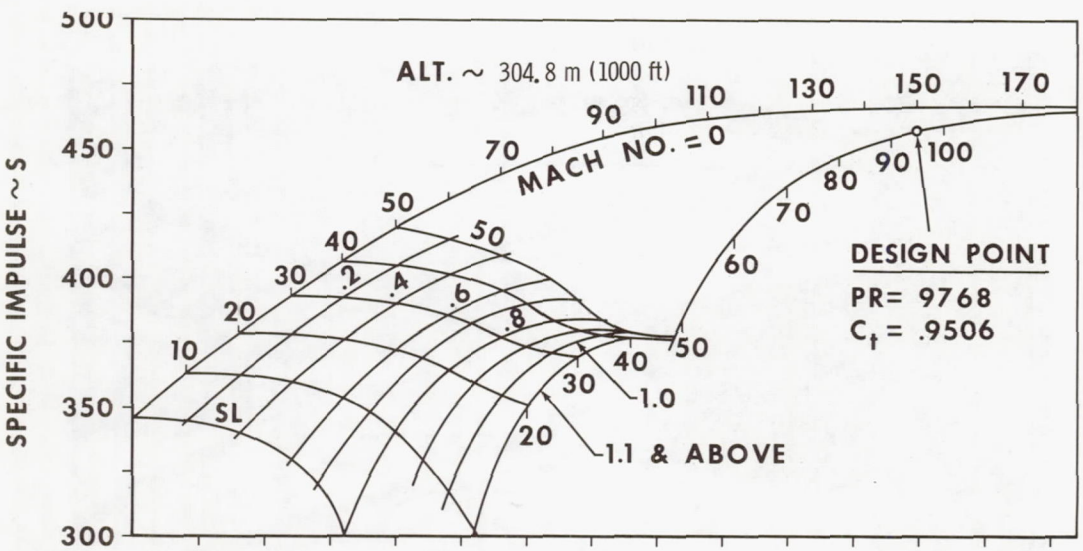

Figure 25. SERV nominal performance of design-point engine ($\epsilon = 433.7$).

interpolation. It is interesting to observe that this engine operates at the point of wake closure with a specific impulse approximately 50 s lower than it would provide in still air. This great difference, however, is caused by the slipstream effect in connection with the tremendous base area.

CONCLUSIONS

An analytical method to determine the performance of an aerospike nozzle, especially the performance contribution from the base area, has been discussed.

Two different types of operation mode exist. The base pressure follows the ambient state just outside the free jet boundary very closely during the open-wake operation mode, whereas the base pressure remains constant for the closed-wake condition. Several parameters such as the sonic line shape, internal shock, ambient pressure, base bleed, nozzle area ratio, turbulence effects, plug length, and aerodynamic slipstream have an effect on the base pressure.

A comparison between experimental and analytical data in connection with visual flow field observance shows good agreement. The parametric presentation of data allows the determination of individual effects and provides a useful tool for aerospike engine performance prediction and optimization.

BIBLIOGRAPHY

Characteristics of Separated Flow Regions Within Altitude Compensating Nozzles. Progress Report No. 4, Report No. 601-PR-4, Contract NAS8-25601, University of Notre Dame, Notre Dame, Indiana, February 1971.

Characteristics of Separated Flow Regions Within Altitude Compensating Nozzles. Progress Report No. 5, Report No. 601-PR-5, Contract NAS8-25601, University of Notre Dame, Notre Dame, Indiana, May 1971.

Mueller, Thomas J.; Sule, Wayne P.; and Hall, Charles R., Jr.: Characteristics of Separated Flow Regions Within Altitude Compensating Nozzles. Final Report UNDAS TN-029-FR-9, Contract NSR15-004-029, University of Notre Dame, Notre Dame, Indiana, January 1971.

Single-Stage Earth-Orbital Reusable Vehicle, Space Shuttle Feasibility Study. Final Report, Contract NAS8-26341, Chrysler Corporation, Space Division, New Orleans, Louisiana, June 30, 1971.

Page intentionally left blank

EXTENDIBLE ROCKET NOZZLE DEVELOPMENT

By

Don Pryor

The extendible rocket nozzle effort at MSFC was an outgrowth of the J-2X experimental engineering program that was active in 1967. The J-2X program investigated a number of improved features for possible incorporation into an advanced version of the Saturn S-IC J-2 engine. The J-2 engine is used as the primary propulsion system for the S-II and S-IVB stages of the S-IC launch vehicle. As depicted in Figure 1, the J-2X program had as a primary objective the evaluation of J-2 engine modifications that would simplify operation and improve reliability. As a secondary objective, the program also investigated methods of increasing thrust without extensively modifying the S-II or S-IVB stages. A thrust increase was achieved by raising engine combustion pressure through a redesign of the engine thrust chamber and propellant feed system.

With the chamber pressure raised to a higher level on an engine that was already operating at an underexpanded nozzle area ratio, the addition of a nozzle extension had obvious thrust improvement possibilities. This concept was, however, restricted in its application to the S-IVB stage of the S-IC launch vehicle. This stage utilizes a single J-2 engine installation, while the S-II stage has five J-2's clustered in such proximity that any additional length-diameter growth is impossible from an engine-to-engine interference standpoint. To accomplish a J-2 engine area ratio increase without violating the interstage confines of the existing S-IVB stage, a movable nozzle extension was required that could be stored about the existing J-2 nozzle before stage separation and translated axially to the full nozzle expansion ratio just prior to S-IVB stage ignition.

Quite early in the evaluation of the J-2X extendible nozzle concepts, the general features listed in Figure 1 were recognized as being worthwhile for application to any upper stage engine. The performance improvement is the most impressive gain realized by adding the additional area ratio for expansion of exhaust gases at vacuum flight conditions. Also, the capability of operating the engine at sea level conditions, with the nozzle extension removed, offers a significant cost reduction feature to an engine development program by removing the requirement of expensive vacuum test facilities

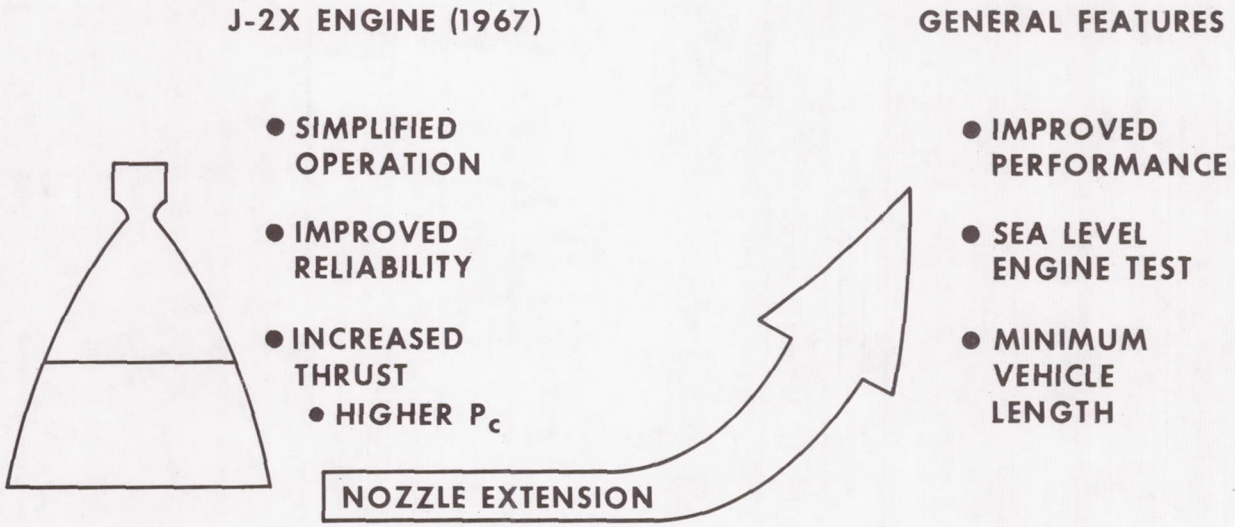

Figure 1. *Extendible nozzle concept evolution.*

during preflight testing. A reduction in vehicle length is realized because of the efficient packaging effect realized by stowing the nozzle around the basic thrust chamber until upper atmosphere engine operation is required.

Figure 2 shows the primary candidate nozzle extension configurations considered by the J-2X program. The design approach to all configurations was limited by several basic constraints, which are listed as ground rules in Figure 2. By far the most influential constraint was the requirement that the extension not violate the basic storage envelope provided for the conventional J-2 installation within the S-IVB engine compartment. This constraint called for ingenious design techniques to stow the additional nozzle length while allowing reliable deployment to the full extension area ratio within a 2-s actuation time.

The Airmat concept shown in Figure 2 is an inflatable extension skirt design that is fabricated from a woven wire structure manufactured by the Goodyear Aerospace Corporation. This concept features a nozzle skirt wall fabricated from two layers of conventionally woven, stainless steel wire yarn with the layers being loosely tied together by a number of interwoven wire yarn strands 10.2 cm (4.0 in.) in length. These strands hold the two wire-cloth layers from expanding outward when pressurizing gas is fed between them. The resulting effect when pressurized is a 10.2-cm (4.0-in.) thick wall that exhibits a high resistance to bending moments when fabricated into the integral cone frustum of the nozzle extension. When unpressurized, the Airmat extension is flexible and can be folded or rolled around the existing J-2 nozzle for storage within the S-IVB interstage. The inflation gas for pressurizing the wall structure comes from

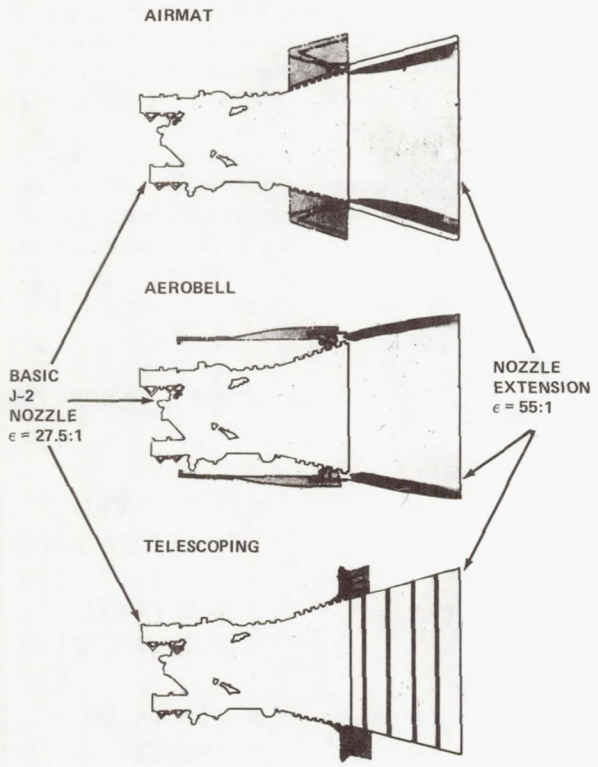

- INFLATABLE SKIRT
- WIRE-WOVEN CONSTRUCTION
- TRANSPIRATION COOLED BY TURBINE EXHAUST

- TRAVERSING SKIRT
- REFRACTORY MATERIALS
- FILM COOLED BY TURBINE EXHAUST

- MULTISECTION TRAVERSING SKIRT
- REFRACTORY MATERIALS
- RADIATION OR TURBINE EXHAUST GAS FILM COOLING

GROUND RULES

- HARDWARE WEIGHT LIMITED TO 340 kg (750 lb)
- PACKAGED WITHIN S-IVB INTERSTAGE
- 2 s ACTUATION TIME

PREDICTED GAINS

- 10 TO 11 s I_{sp}
- 1452 TO 1905 kg (3200 TO 4200 lb) PAYLOAD (MINUS SYSTEM WEIGHT)

Figure 2. J-2X extendible nozzle concepts.

the J-2 turbine exhaust products that are normally dumped into the main exhaust stream through a ring of orifices around the basic J-2 nozzle.

As in any woven product, the Airmat exhibits a matrix of fine openings between the woven yarn filaments that make up the two wire-cloth face layers. This porosity is utilized on the inner nozzle face, next to the hot main chamber combustion flow, to allow the turbine exhaust pressurizing gas to escape from the nozzle extension and perform a transpiration cooling function in the process. The external wall is sealed to prevent escape of the pressurizing gas.

Actuation of the Airmat extension is automatic, with turbine exhaust flow providing the driving force to deploy the folded material to the fully extended position. Overall system weight estimates, including the turbine exhaust ducting and manifold, nozzle attachment fixtures, etc., indicate that the Airmat extension assembly will weight 204.12 kg (450 lb).

The Aerobell nozzle extension concept of Figure 2 required a single piece, truncated cone fabricated from refractory materials. It was to be mechanically actuated from its stowed position about the basic J-2 nozzle cone by eight pneumatic motors driving collapsible struts. These collapsible struts were to be fabricated from flexible steel tubing that would fold into a flat ribbon about a storage drum and expand into a rigid columnar strut upon being unrolled from the drum. Nozzle cooling was to be accomplished by dumping the turbine exhaust flow in at the extension attachment plane through a 360-deg circumferential slot. This flow would provide a protective film coolant boundary layer along the extension wall. This concept was estimated to have total assembly weight of 249.48 to 272.16 kg (550 to 600 lb).

The third configuration shown in Figure 2 was a telescoping extension concept composed of five truncated cone segments that nested one within another in the stowed position about the J-2 basic nozzle. These segments were linked together by six sets of spring-loaded scissor arm mechanisms. The extension was to be stored with the spring-loaded arms compressed so that the deployment command released them to actuate the conical segments to the fully extended position. In reaching the extended position, the scissor arm assemblies moved past center and mechanically locked into a compression-carrying member that was capable of transmitting the extension thrust into the basic nozzle. Cooling would be by radiation or film using the turbine exhaust products in a manner similar to the Aerobell concept. A circumferential seal was required at each of the four joints between the five extension segments, and a total assembly weight of 192.78 kg (425 lb) was predicted

The J-2X program was canceled prematurely, leaving the nozzle extension concepts only partially evaluated. Based on the impressive benefits for engines in general shown in Figure 1, a decision was made to continue the evaluation of at least one of the three concepts of Figure 2 under research technology sponsorship. Since the Aerobell concept with its mechanically driven, single-piece skirt was very similar in concept to the LR-129 research engine already under test by the Air Force, this concept was eliminated from further consideration. The telescoping extension had already been modeled in full scale on a nonoperational J-2 engine to demonstrate the acutation characteristics of the spring-driven scissor arm mechanisms. The results of this modeling effort were encouraging, but the complexity of the multiple-section telescoping assembly was overriding and the evaluation was discontinued. The Airmat extension concept with its competitive light weight and attractive simplicity was therefore selected for further study.

The Airmat extension is fabricated, as mentioned earlier, from a woven wire structure that is woven on looms that are somewhat conventional (Fig. 3). Figure 4 is a cross section of the nozzle wall structure showing the two face plys connected by the interwoven drop cords. The pressurizing/cooling medium is shown to be sealed from ineffectual escape through the outer wall face ply by a silicon rubber coating bonded to the external wall surface. The yarn used to weave the wall material was twisted from filaments of 1.27×10^{-5} m (0.5 mil) stainless steel (type 304) wire, and the finished material has a highly pliable quality quite similar to woven textile products. This flexible nature makes the stowage design for the conical extension about the basic J-2 engine nozzle highly practical. It also improves the likelihood of reliable deployment from the stowed to the extended position solely by the turbine exhaust pressurization transient.

Before these features of stowage and deployment could be investigated, the more basic design considerations of Figure 5 had to be made compatible. These parameters are each interrelated and highly

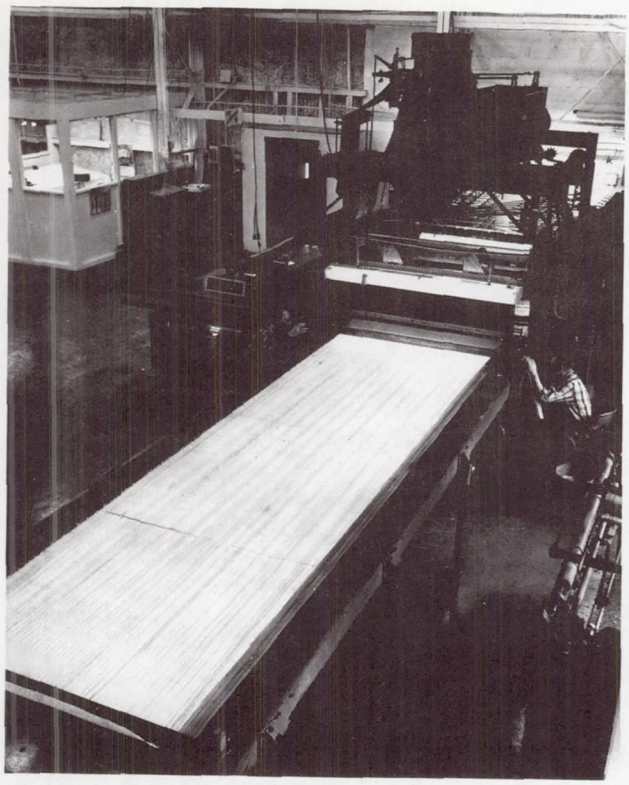

Figure 3. Looms used for weaving wire structure.

dependent on one another, and the design process consisted of a series of compromises aimed at providing the maximum performance improvement available for the given operating conditions.

The two biggest interrelated parameters of the inflatable nozzle design were the coolant gas conditions and nozzle wall inflation pressure. In the subject design application, the coolant gas supply conditions from the turbine exhaust of the J-2 engine were fixed and could not be modified without throwing the engine system operation out of balance. This left the nozzle wall pressure and the parameters influencing it as the design variables.

Of primary consideration to the concept design was just how large an expansion ratio/performance increase could be provided with the given coolant/pressurization gas flows. Figure 6 shows the relationship of internal Airmat wall pressure versus nozzle expansion ratio for various families of wall porosity and structural load carrying capability. The structural load curves indicate the minimum wall pressure required to maintain structural integrity for a nozzle of the desired area ratio. The various factors of structural load (1.0 through 1.5) represent multiples of the basic stress imposed by main engine exhaust gas pressure, friction drag, etc., acting on the nozzle extension.

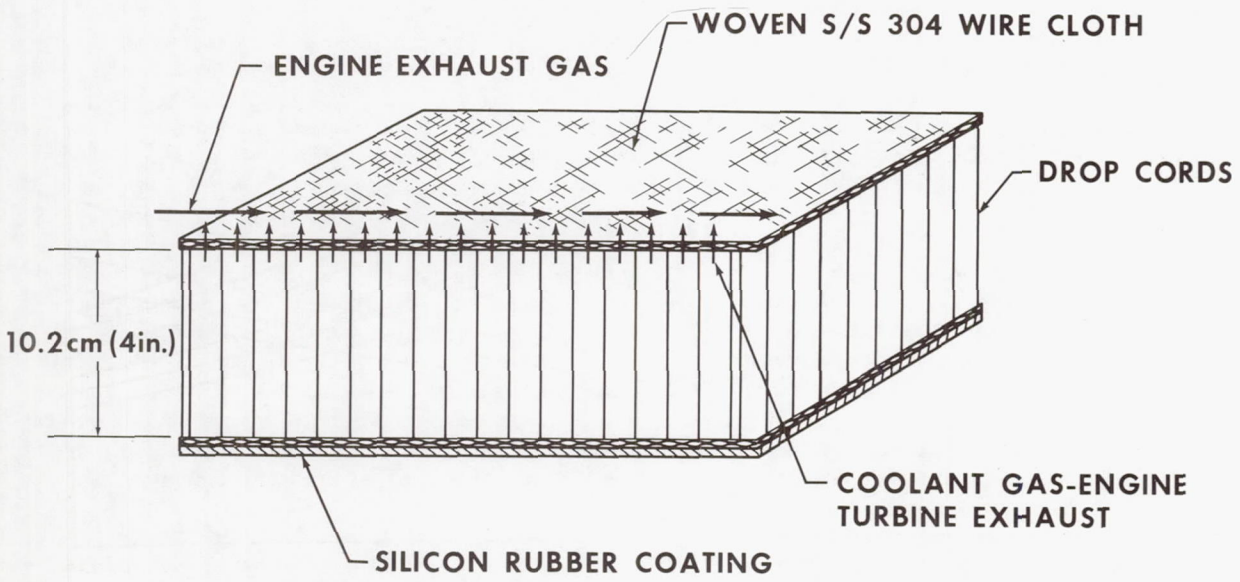

Figure 4. Airmat inflatable nozzle extension wall structure.

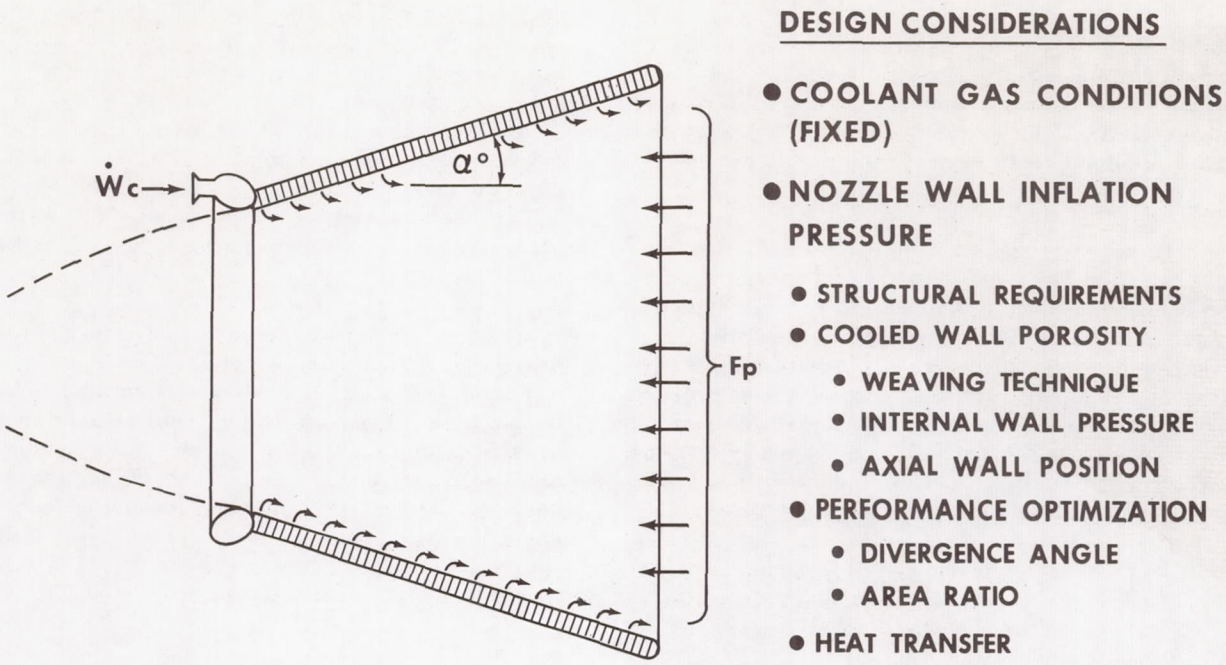

Figure 5. Extendible rocket nozzle development.

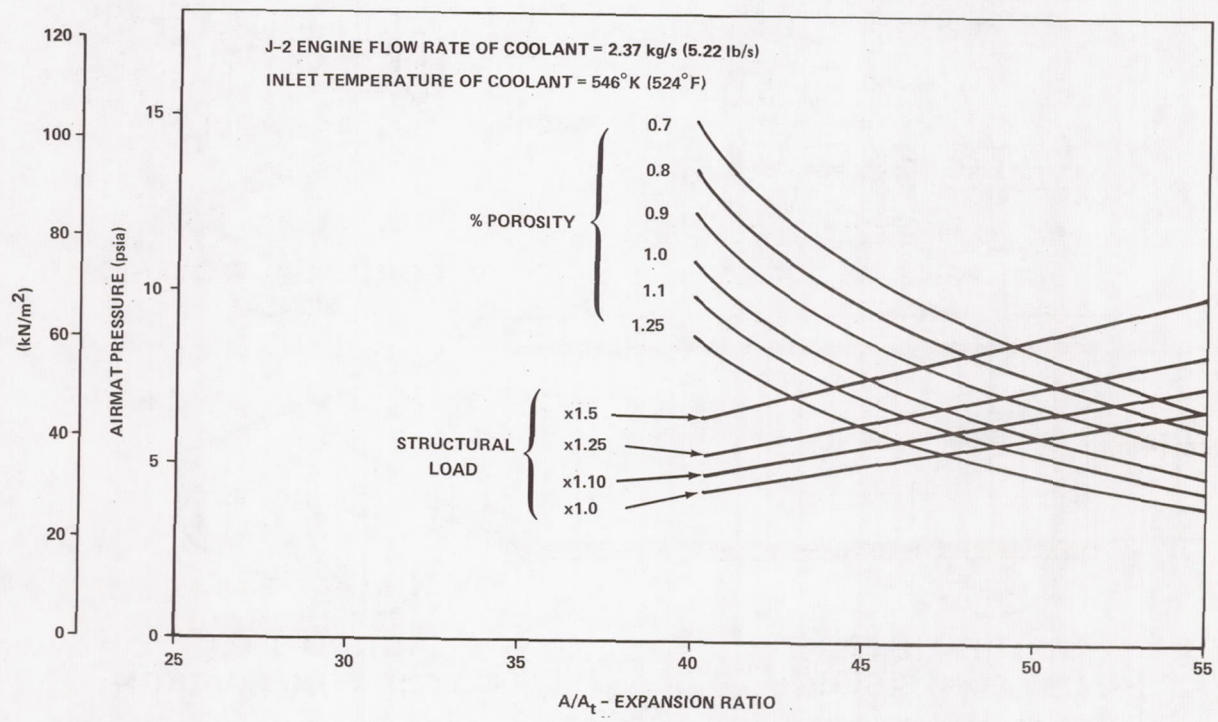

Figure 6. Airmat pressure versus nozzle extension expansion ratio.

The percent porosity curves show a decreasing internal wall pressure, as would be expected to result from increasing the area ratio and consequently the wall surface area/cooling flow openings. Wall porosities ranging from 0.7 to 1.25 were predicted as reasonably achievable for the woven-wire Airmat.

The porosity value of the Airmat wall was dependent on the weaving and nozzle construction technique as shown in Figure 7. The wall material could be woven in flat panels which simplified the weaving process and improved porosity control but greatly complicated the nozzle construction process. With flat panel woven Airmat for a raw material, the conical nozzle form had to be shaped by appropriate cutting, splicing, and seaming operations. A true conical frustum was difficult to control using this construction method. If however, the basic Airmat wall was woven in a manner such that the material advanced from the loom at an unequal rate across its outlet, the resulting effect was a curled panel that could be joined at one seam to produce the desired cone frustum shape. Porosity was affected by the uneven feed rate from the loom such that the slower advancing material achieved a tighter, less porous weave while the higher advance rate material from the loom was less dense and more porous. This porosity variation, while undesirable, was not considered serious with variations only amounting to 0.2 percent.

Other considerations listed in Figure 5 that affect wall porosity are the internal wall pressure and axial wall position at which the porosity is being evaluated. The porous Airmat wall tends to stretch when pressurized, thereby spreading the openings between the woven yarn and increasing the effective porosity. In regard to the axial position of measured porosity, there is likely to be a slight inner wall pressure drop between the end that is attached to the basic J-2 nozzle and the exit end of the

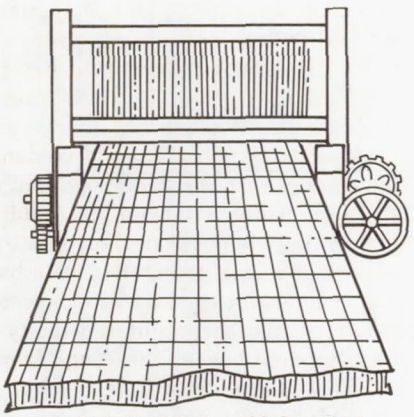

FLAT PANEL WOVEN AIRMAT

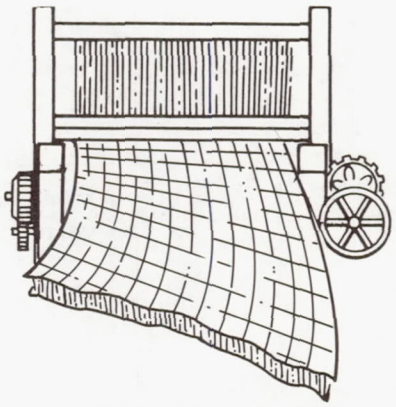

CONICALLY WOVEN AIRMAT

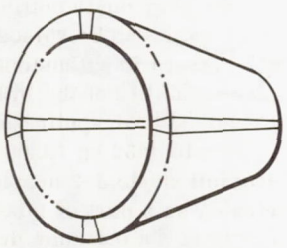

MULTIPANELED NOZZLE CONSTRUCTION

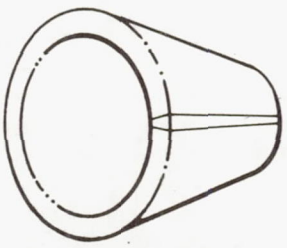

SINGLE PIECE NOZZLE CONSTRUCTION

Figure 7. Airmat woven wall construction techniques.

extension. This internal pressure decay down the nozzle length would tend to close somewhat the effective porosity resulting from the aforementioned stretching phenomena of the Airmat structure under inflation.

The design considerations of Figure 5 included the performance optimization aspects for the nozzle extension. Figure 8 illustrates the gain in engine specific impulse resulting from increasing the area ratio by multiples of some basic expansion ratio (ϵ). For purposes of illustration, this basic expansion ratio (ϵ) was identified as that nozzle exit area which would flow full, without separation, at a sea level back pressure. Figure 8 shows the increase in engine specific impulse above the sea level delivered value (expansion ratio = ϵ) when the nozzle expansion ratio is increased to some new level (ϵ') and operated at vacuum back-pressure conditions. This relation is a function of engine chamber pressure, and three different pressures are plotted in Figure 8. Divergence angle as well as area ratio must be optimized as a part of the performance optimization step of the design process.

The final area of discussion from the design considerations of Figure 5 is heat transfer. Because of the criticality of the transpiration cooling concept for the Airmat nozzle extension, an experimental evaluation was conducted. Figure 9 shows the experimental Airmat extension in place and inflated in a model test engine facility. The model test engine was a 17 792-N (400-lb) thrust, lox/GH_2 engine operating at 586 N/cm^2 (850 psia) chamber pressure.

The Airmat nozzle extension was attached to the existing engine nozzle at an area ratio of 27:1 and extended the expansion ratio to an 80:1 value. To provide the required 80:1 expansion ratio test capability, the nozzle extension was operated in a self-pumping diffuser that was removed in Figure 9 to expose the nozzle. The nozzle extension was inflated and transpiration-cooled with heated hydrogen gas in an attempt to duplicate the turbine exhaust products from the J-2 engine. The major constituent of the J-2 engine exhaust gas is hydrogen at a temperature of nearly 589°K (600°F). This temperature could not be modeled by the hydrogen pressurant used in the test program, since the facility could only provide 422°K (300°F) hydrogen at the required flow rates.

Testing was conducted over a range of inflation/coolant inlet flows and temperatures and the data are plotted over curves of theoretically predicted nozzle extension wall temperature versus coolant flow rate in Figure 10. The major conclusion from the experimental data was that the theoretical predictions of wall temperature versus coolant flow/temperature conditions are conservative. The theory expressed in Figure 10 shows a strong increase in the nozzle wall temperature as the coolant flow is reduced. The test data agreed fairly consistently with the theoretical data except that the reduced coolant flow of tests A and B failed to drive the wall temperature up the theoretical curve for coolant temperatures of 422°K (300°F). A projection of these data to the J-2 application is shown in Figure 11.

Figure 11 plots theoretical J-2 nozzle extension wall temperature adjusted by the test data of Figure 10. The temperature predictions are made for the extension wall at the plane of attachment to the fixed J-2 nozzle exit. This plane of the nozzle extension is under the most severe heating environment, not only from the worst case conditions of the main engine exhaust flow but from the lack of any protective boundary layer from upstream transpiration-coolant flow. Even with these severe conditions, the wall temperature is seen to range from only 533 to 755°K (500 to 900°F) depending on the selected nozzle extension expansion ratio and coolant flow rate. The range of coolant flows is that associated with the J-2 propellant utilization (PU) system which balances fuel/oxidizer flow so that propellant residuals in the vehicle tanks may be minimized at engine cutoff. This balancing process is accomplished by varying the amount of turbine drive gas that would eventually be fed to the nozzle extension; hence, the range from 2.04 to 2.95 kg/s (4.5 to 6.5 lb/s).

The end product of this study is illustrated in Figure 12. The J-2 engine with the nozzle extension is shown in both the retracted and extended positions. As optimized by the previously outlined design process, the area ratio can be raised from 27.5:1 to 48:1. Higher area ratio extensions are limited by the structural capability of the inflated assembly. Payload gains predicted for application to a J-2/S-IVB stage amount to 1452 kg (3200 lb). Figure 13 shows one of two full-scale J-2 nozzle extensions that were fabricated as a part of this effort. One unit was fabricated at the optimum design expansion ratio of 48:1, while the other was fabricated at a more conservative 41.3:1 expansion ratio. It was originally intended to fire the J-2 engine with first the 41.3:1 extension and then the 48:1 unit within the altitude facilities of Arnold Engineering

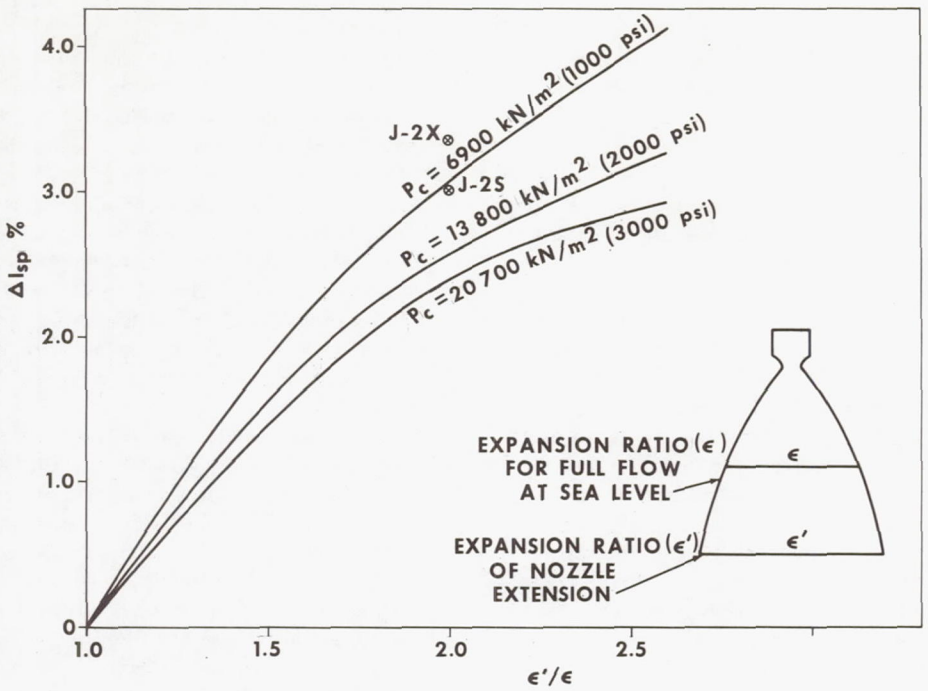

Figure 8. Theoretical performance gain for expansion below sea level pressure.

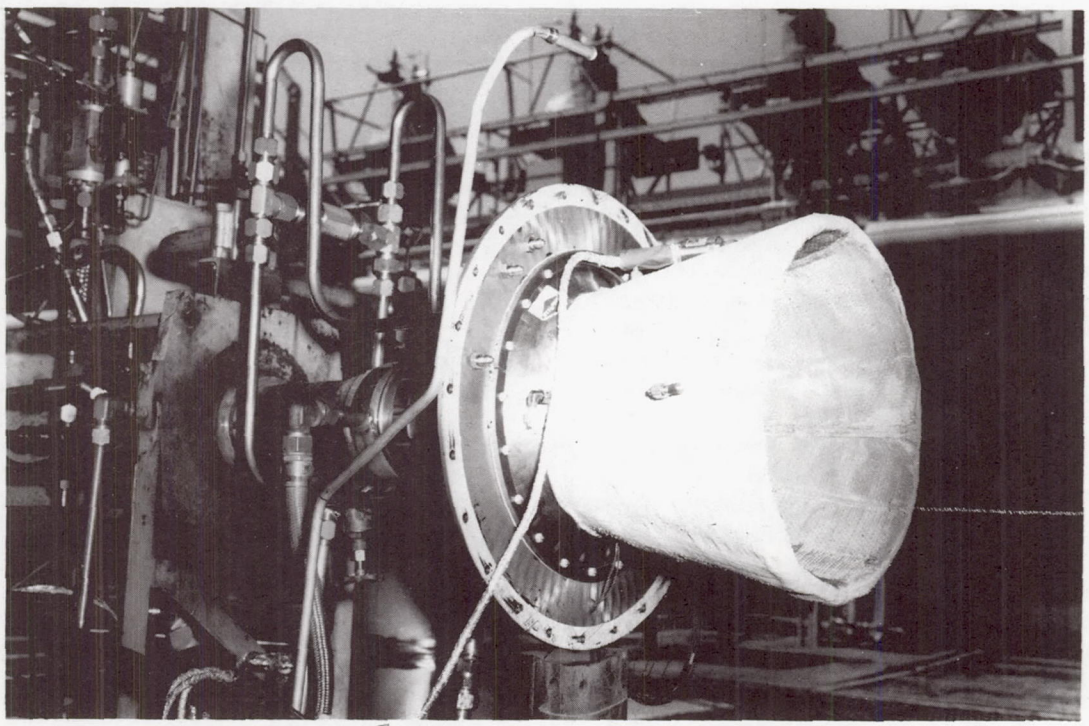

Figure 9. View of Goodyear nozzle setup.

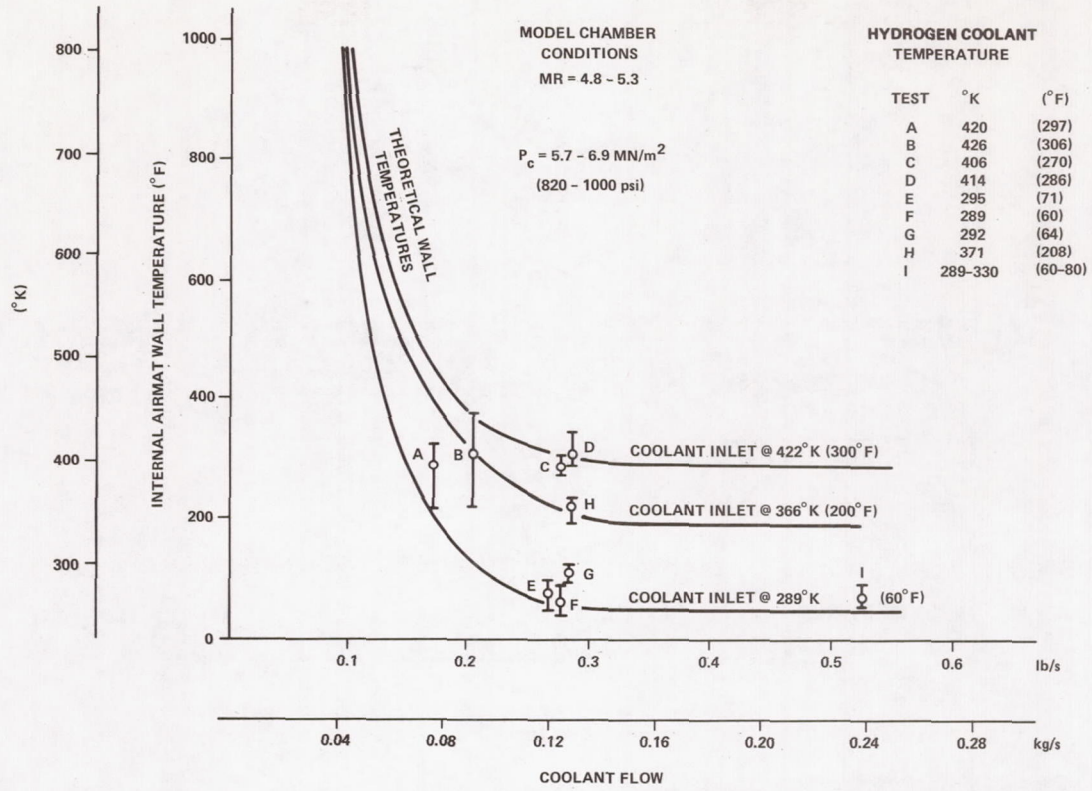

Figure 10. Model extension test data.

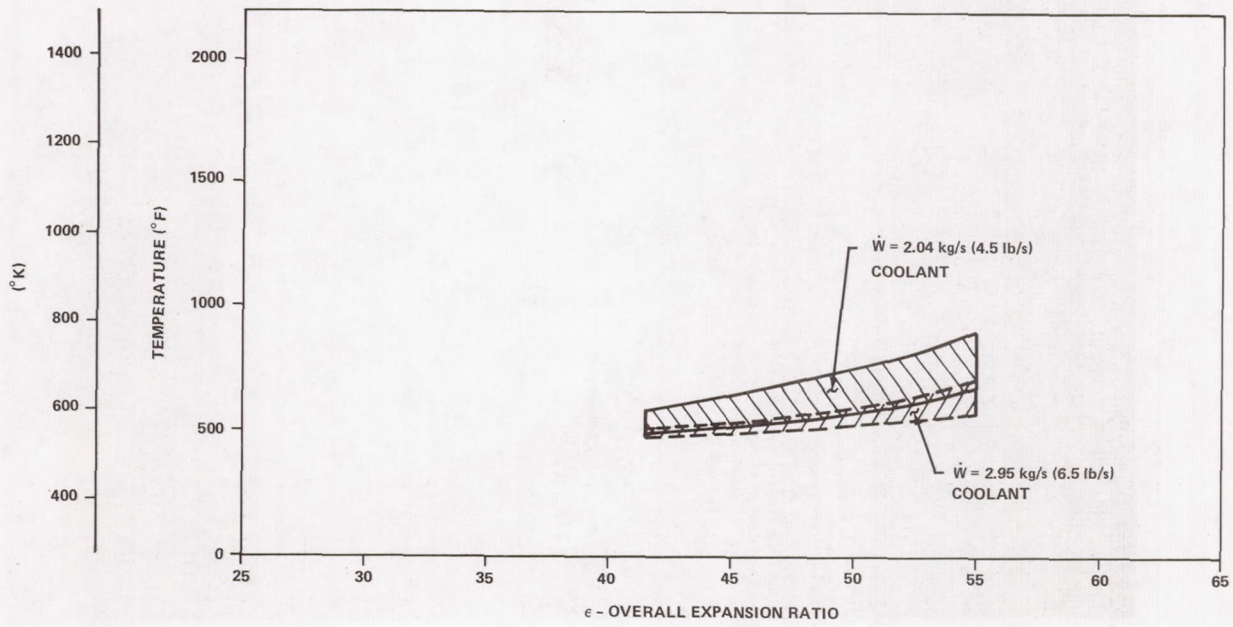

Figure 11. Theoretical nozzle extension surface temperature at attachment point (ϵ = 27.5:1) for varying overall expansion ratios.

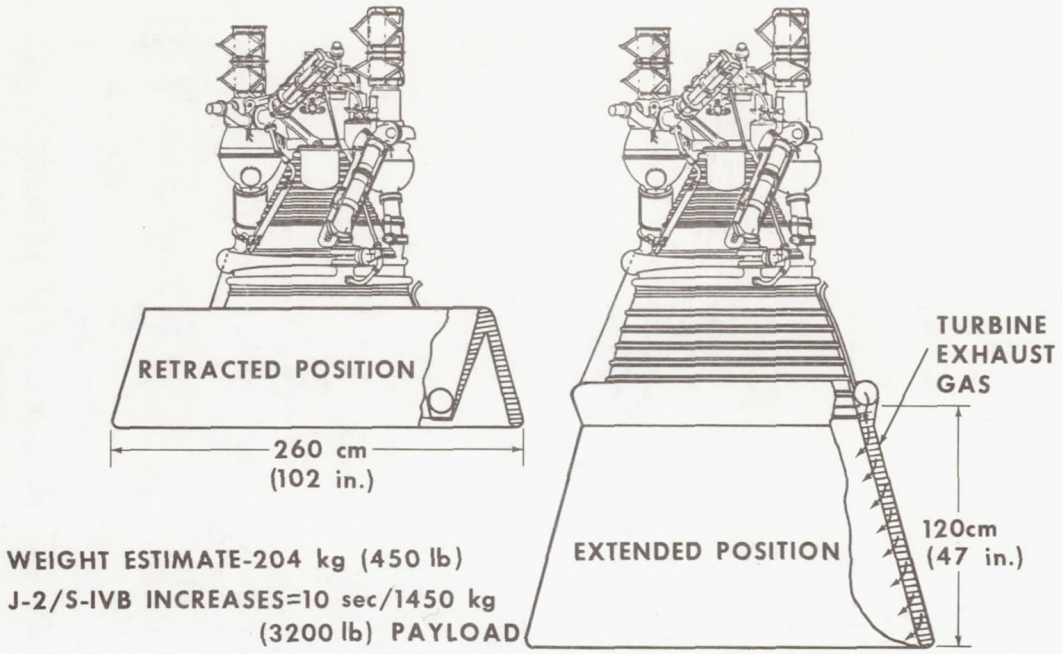

Figure 12. Airmat inflatable nozzle — J-2 application.

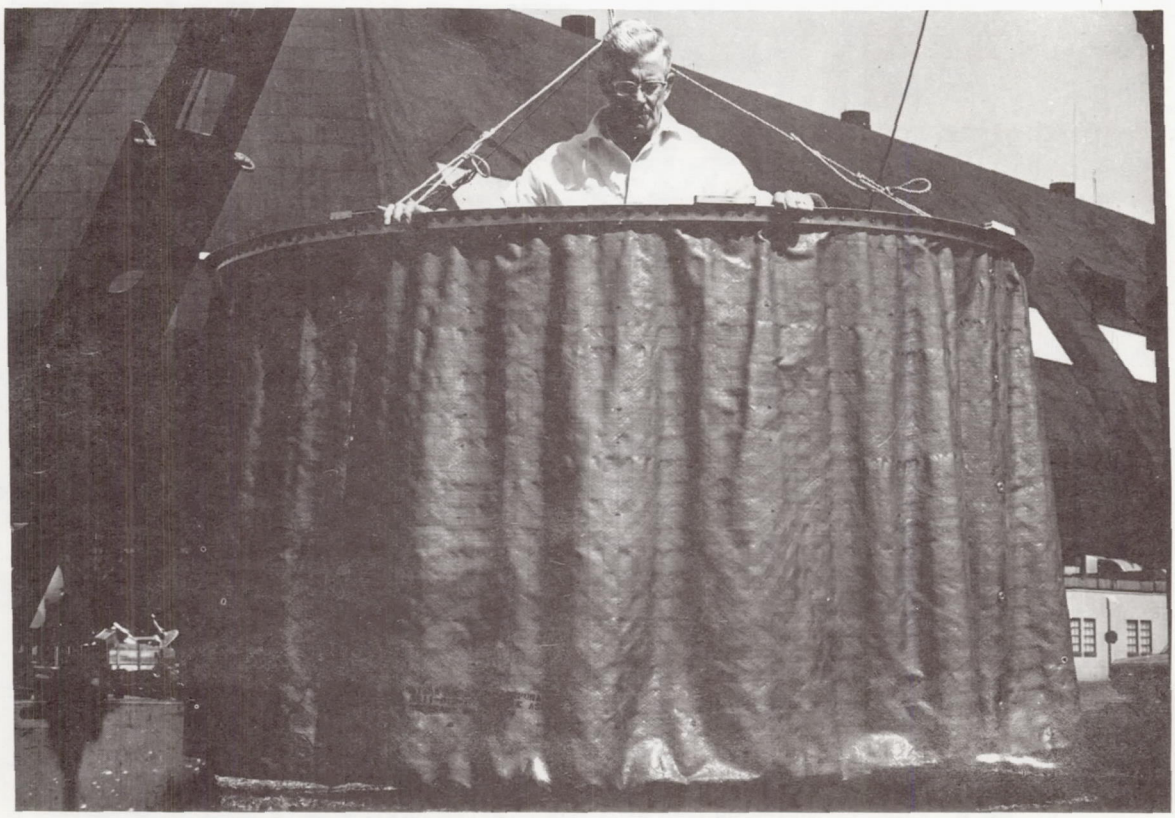

Figure 13. Long nozzle.

Development Center, but the J-2 engine firings at that facility were prematurely canceled before fabrication of the nozzle extensions could be completed. However, the fabrication program was completed in order to gain the valuable weaving and nozzle cone fabrication technology necessary to evaluate the concept for any future application. In addition, an inflation/deployment test series is scheduled to be conducted at MSFC using the full-size nozzle extensions. This test series will subject the extensions to the design inflation pressures and transients predicted for actual J-2 operation but will use a cold gas (GN_2) inflation source on an inoperative J-2; i.e., no main chamber exhaust products passing through the nozzle extension. Also, as a part of the testing, the extension will be stored in its retracted position, similar to the concept of Figure 12, and will be actuated by internal pressurization to the fully extended position. The test series will include appropriate instrumentation and filming to demonstrate the extension deployment process and fully inflated nozzle shape.